Chem Soc Rev

The importance of hydration and DNA conformation in interpreting infrared spectra of cells and tissues

Journal:	*Chemical Society Reviews*
Manuscript ID	CS-REV-06-2015-000511.R3
Article Type:	Review Article
Date Submitted by the Author:	15-Sep-2015
Complete List of Authors:	Wood, Bayden; Monash University, Department of Chemistry

The importance of hydration and DNA conformation in interpreting infrared spectra of cells and tissues

Bayden R. Wood

Centre for Biospectroscopy, School of Chemistry, Monash University, 3800, Victoria, Australia

Abstract

Since Watson and Crick's historical papers on the structure and function of DNA based on Rosalind Franklin's and Maurice Wilkin's X-ray diffraction patterns tremendous scientific curiosities have been aroused by the unique and dynamic structure of the molecule of life. A-DNA and B-DNA represent different conformations of the DNA molecule, which is stabilised by hydrogen interactions between base pairs, stacking interactions between neighboring bases and long-range intra- and inter-backbone forces. This review highlights the contribution Fourier transform infrared (FTIR) spectroscopy has made to the understanding of DNA conformation in relation to hydration and its potential role in clinical diagnostics. The review will first begin by elucidating the main forms of DNA conformation found in nature and the general structures of the A, B and Z forms. This is followed by a detailed critique on infrared spectroscopy applied DNA conformation highlighting pivotal studies on isolated DNA, polynucleotides, nucleoprotein and nucleohistone complexes. A discussion on the potential of diagnosing cancer using FTIR

spectroscopy based on the detection of DNA bands in cells and tissues will ensue, highlighting the recent studies investigating the conformation of DNA in hydrated and dehydrated cells. The method of hydration as a way to facilitate DNA conformational band assignment will be discussed and the conformational change to the A-form upon dehydration will be used to explain the reason for the apparent lack of FTIR DNA signals observed in fixed or air-dried cells and tissues. The advantages of investigating B-DNA in the hydrated state, as opposed to A-DNA in the dehydrated state, are exemplified in a series of studies that show: 1) improved quantification of DNA in cells; 2) improved discrimination and reproducibility of FTIR spectra recorded of cells progressing through the cell cycle; 3) insights into the biological significance of A-DNA as evidenced by an interesting study on bacteria, which can survive desiccation and at the same time undergo the B-A-B transition. Finally, the importance of preserving the B-DNA conformation for the diagnosis of cancer is put forward as way to improve the sensitivity of this powerful technique.

A, B and Z-like DNA in nature

DNA can assume many different helical forms with the main families being right-handed A- and B-DNA and left-handed Z-DNA helices. A-DNA, forms within specific stretches of purines (GAGGGA); B-DNA, is generally characterised by mixed sequences, and Z-DNA is favoured by alternating pyrimidine–purine based (CGCGCG).[1] The majority of DNA found in functional cells is mainly in the B-like form but alternative DNA structures can exist in both prokaryotic and eukaryotic cells.[2] An *en masse* DNA conformation can be induced by a number of factors including base composition,[3] water content,[4] salt concentration[5] and the species of the counter ion.[6] The more common B-DNA form in living cells can also undergo local

structural transitions into other DNA forms that can be functionally important.[2] Several lines of evidence indicate that non-B-DNA forms exist within specific sequences of DNA, which can be induced by changes in environmental conditions, protein binding, RNA binding and superhelical tension.[2] Repetitive DNA motifs may fold into non-B DNA structures such as left-handed Z-DNA, cruciforms, intramolecular triplexes, quadruplex DNA, parallel-stranded DNA, slipped-strand DNA and unpaired DNA structures.[7, 8]

A-like DNA is the conformation adopted under relative low water content (<75% r.h. for NaDNA) but its formation is also strongly dependent on base composition[1] and environmental factors like pH,[9] salt concentration[5] and counter ion influence.[10] Early studies by Rich[11] demonstrated that RNA and DNA formed complexes but they had no direct experimental information at that time suggesting that DNA nucleotide sequence influences the ordering of the nucleotides on RNA. X-ray diffraction patterns of the sodium salt of a DNA-RNA hybrid prepared from single-stranded fibre of DNA showed that the hybrid possesses a helical conformation almost identical to the A-form of sodium DNA, which differed from double-helical RNA.[12] However, B-forms and other DNA-RNA hybrid conformations can result depending on the specific base sequences.[1] The only differences between the chemical structures lay in the absence of the 5-methyl group on the uracil and the presence of a 2'-hydroxyl group on the ribose of the RNA strand.[12] This indicated that the 2'-hydroxyl is probably responsible for the difference in behavior between DNA and the DNA-RNA hybrid.[12] Milman et al.[12] built molecular models that demonstrated that the 2'-hydroxyl group could not be accommodated into the B-form of DNA without considerable distortion, but no major steric problems are created by the addition of a 2'-hydroxyl group to the sugar residue of DNA in the A-form. This fundamental

attraction in the hybrid DNA-RNA helix and its resultant conformation remains the foundation for information transfer in biological systems.[13]

Using circular dichroism Fairall et al.[14] identified specific sequences of poly(dG). poly(dC) formed an A-like helix. It would therefore seem reasonable that short sequences of DNA in living organisms would have sections of A-DNA. In general polynucleotides with high guanine often crystallize to an A-like helical form, and are thought to exist in both a B- to A-DNA transition in solution. Burckhardt et al.[9] monitored the course of complex formation of DNA with poly-L-histidine and through pH manipulation demonstrated three different conformational states that could be reversed from B- to A-DNA to form a condensed phase containing a mixture of B-type or possibly C-type structures. A-like DNA conformations result upon the binding of specific proteins and may be an important intermediate step in formation of strongly distorted DNA conformation observed upon binding with proteins.[15, 16] It has been suggested that small regions of DNA are in an A-like conformation *in vivo* thus facilitating interaction with specific proteins.[17-19] Nanosecond scale molecular dynamics simulations of the DNA oligomer, 5'-GCGTATATAAAACGC-3' in water, which contains a target site for the TATA-box binding protein (TBP) was shown to adopt an A-like conformation and undergoes bending related to that seen within the complex with the TBP.[17] This is consistent with A-DNA being an important intermediate step in forming a strongly distorted DNA structure observed within its complex with TBP in crystals.[18] Crystallographic studies have identified a polymerase-induced A-DNA conformation in HIV reverse transcriptase bound to DNA.[19] It is thought that the A-DNA in the vicinity of the DNA polymerase active site may improve the base pair fit in the template-primer duplex increasing the reliability of the proofreading and the accuracy of the synthesis.[16] The *Escherichia*

coli cyclic adenosine monophosphate receptor protein (CAMP) induces DNA bending with DNA remaining in the B-form when the spacer in the sequence TGTGANNNNNTCACA (where N is either T,C,G or A) in 6 bp but changes to the A-form with an 8 bp spacer in order to shorten the distance between TGTGA sites for CAMP binding. The conformational change from the A-B form on protein binding to DNA in *Bacillus* spores may confer resistance to Ultra Violet (UV) damage because of the fact that nucleobases of A-DNA are less susceptible to UV damage compared with B-DNA.[2] A group of small, acid-soluble spore proteins (SASP) of the α/β -type are thought to play an important role in the formation of A-DNA.[20] Analyses using circular dichroism and Fourier-transform infrared spectroscopy confirm binding of α/β -type SASPs to DNA *in vitro* causes a structural change in DNA, from the B to the A conformation, which provides the basis whereby α/β-type SASPs confer increased spore UV resistance *in vivo*.[20] By changing spore DNA conformation, the DNA photochemistry is altered in such a way that UV irradiation produces spore photoproduct instead of the more lethal cyclobutane-type thymine dimers.[20] Recently the DNA in the rod-shaped virus SIRV2 (*Sulfolobus islandicus* rod-shaped virus 2), which infects the hyperthermophilic acidophile *Sulfolobus islandicus* and lives at 80°C and pH 3 was found to exist entirely in the A-form, indicating a common mechanism with bacterial spores for protecting DNA in the most adverse environments.[21] From recent FTIR studies it would appear the A-DNA conformation plays a critical role in protecting bacteria from desiccation as their DNA can undergo an *en masse* B-A-B-transition and still produce progeny as will be discussed.[22]

Evidence for a left-hand helical form of DNA, namely Z-DNA, came from Pohl and Jovin[23] who recorded ultraviolet circular dicrohism (CD) of poly(dG-dC) and showed that the CD spectrum was nearly inverted in 4 M sodium chloride solution. The

hypothesis that there was a conversion from B-DNA to a left-handed helical form Z-DNA was confirmed by examining the Raman spectra of the solutions and Z-DNA crystals.[24] The first single-crystal X-ray structure recorded of a DNA fragment d(CG)3 showed a left-handed double helix with two anti-parallel chains that were held together by Watson–Crick base pairs. It was found that sequences that most readily converted to Z-DNA had alterations of purines and pyrimidines and especially alternations of C and G. Alternations of CA on one strand and TG on the other also formed Z-DNA conformations but many other sequences were shown to be capable of forming Z-DNA.[25] Z-DNA is highly antigenic, and unlike DNA, antibodies can be raised to Z-DNA molecules.[25] The identification and characterization of these antibodies led to the discovery that Z-DNA-specific antibodies are found in human pathological conditions like systemic *lupus erythematosus,*[26] Huntington's chorea, Fragile X-syndrome and patients severely affected by Alzheimer's disease.[27]

It should be noted that such local changes in site-specific sequences are unlikely to be directly detected by FTIR in cells and tissues and really only gross changes that cause an *en masse* change are potentially detectable with the technique. Emerging near-field technologies such as Tip Enhanced Raman Scattering (TERS)[28] and Nano-infrared spectroscopy[29] would have the spatial resolution to investigate site-specific sequences in plasmid DNA. Indeed TERS has shown promise to detect probe single bases of DNA[30] and double and single strand breaks in plasmid DNA exposed to UV light.[31]

Structure and dynamics of DNA conformations

DNA has a nearly regular structure based on a sugar-phosphate chain skeleton with an accurately repeating pattern of atoms along the chain. In physics it is known as a one-dimensional crystal but has properties more akin to a polymer including structural

flexibility with the ability to bend, turn and change conformation.[32] Table 1 shows the important structural parameters for the A, B and Z-DNA conformations. In terms of structure A-like DNA, is narrower and is characterized by more base pairs per turn of the helix and a wider minor groove than B-like DNA. B-DNA has a 10.5-fold screwed symmetry and a pitch of 3.4 nm (distance between base pairs), while A-DNA is more compact with a pitch of 2.82 nm and a 12-fold symmetry. Z-DNA is a left-handed helical form with a 6-fold symmetry and a pitch of 4.4 nm.[33] The critical distances and interpretation of the B-form helix was born out of the interpretation of the crystal structure shown in Figure 1, which shows how the reciprocal distances and angles of the crystal structure relate to the B-form conformation in this case.

Z-DNA can form in alternating purine-pyrimidine sequences under certain conditions, including high salt concentration and in the presence of certain divalent cations, or DNA supercoiling.[34] In comparison to B-DNA, the major structural differences occur in the sugar pucker, rotations about the glycosidic bond, and orientation of base pairs within the helix.[34] The structures of these major forms are depicted in Figure 2 and a schematic of the major parameters for B-DNA are shown in Figure 3. A dominant feature of B-DNA is the presence of two distinct grooves, a major and a minor groove, which provide very distinct surfaces with which proteins can interact (Figure 3). In A-DNA, the base pairs are tilted between 13 and 19 degrees from the perpendicular, whereas in B-DNA the inclination is close to zero with the base pairs stacked nearly perpendicular to the helix axis, where the axis runs through the center of each base pair.[35]

Studies have shown DNA to have an incredible degree of conformational flexibility and the number of base pairs per turn is not the same in solution and in fibers.[36] Moreover, the backbone and the base atoms undergo angular motions greater that 25°

in nanoseconds.[37] Model building and computer calculations have considered the static deformation of the DNA double helix by kinking, bending and twisting.[38] Barkley and Zimm[39] applied mathematics to model the dynamic behaviour of DNA by assuming that the molecule behaved like an isotropic elastic rod. DNA is both dynamic and very stable. The stability of the DNA double helix depends on a fine balance of hydrogen bond between other bases and surrounding water molecules, as well as base-stacking interactions between adjacent bases.[32] Small variations in the DNA sequence can have severe effect on the stability of the DNA double helix. Mutations in the base sequence can result in mismatches that lead to unstable duplexes. Proofreading enzymes, which recognize the mutation and replace it with the correct nucleotide, can rectify the instability. Increasing the salt concentration increases the base-stacking interactions because high salt concentrations mask the destabilising charge repulsion between the two negatively charged phosphodiester backbones.[40] The stability of the DNA duplex therefore increases with increasing salt concentration and also the type of counter ion.[40] Divalent cations such as Mg^{2+} are more stabilising than Na^{+} ions, and some metal ions bind to specific loci on the DNA duplex.[40] The improved stability achieved using divalent cations such as Mg^{2+} has enabled researchers to orientate and stabilise plasmid DNA on mica and metal surfaces for Atomic Force Microscopy and near-field spectroscopic measurements.[31]

The dynamical nature of the molecule and its ability to complimentarily bind to other nucleic acids and proteins in nanoseconds, along with its inherent stability and the capability to be proofread, is fundamental to the origin and success of life.

Methods for investigating DNA conformation

The early X-ray experiments on proteins reveal molecular conformations and the α-helix is borne

While Watson and Crick are accredited with proposing the structure[41] and function of DNA[42] a number of critical pieces of evidence led to the elucidation of the helical structure and the important DNA conformations especially from the early X-ray diffraction experiments of proteins and polypeptides. The first studies investigating different conformations of keratin were made by Herzog and Jancke.[43] Pioneering studies by Meyer and Mark in the late 1920s working on natural silk (fibroin),[44] tendon[45] and muscle[45] led them to first discern "globular" protein from so called "fibrillar" proteins. They were also the first to propose a reversible folding and unfolding model for polypeptide chains, which was exemplified by the decrease in viscosity of gelatin approaching the isoelectric point, which they surmised was because of coiling or folding of the protein.[46] Early X-ray diffraction studies on hair by W.T. Astbury, who is known as the father of molecular biology, showed that a different X-ray photograph was produced for stretched (α-photograph) and unstretched hair (β-photograph). In summarizing the results of his classic paper on the X-ray diffraction patterns of wool, hair and related fibres he states. *The whole series of experiments convey the impression of long filament-like molecules, which in some way involve the continuous repetition of hexagonal ring systems connected by bridge atoms.* He proposed three main forms of proteins based on X-ray diffraction patterns namely the α-form (exemplified by upstretched wool), a β-form (as found in stretched wool) and a γ-form attributed to tendon. The α-form corresponded to the proteins he designated K-m-e-f (keratin, myosin, epidermin and fibrinogen)

with strong meridional arcs at 5.15 Å from repeating units within the structure and a group of equatorial reflexions at ~10 Å and 27 Å. Moreover, he demonstrated the α-β transformation in keratin is reversible and appears to be based on the elongation of an intramolecular group of length 5.15 Å to another group of length 6 .64 Å giving a 29 per cent increase. These early X-ray studies stimulated a number of proposed models to deduce the arrangement of the chains. A detailed study by Huggins on fibrous proteins proposed a hypothetical structure composed of spiral polypeptide chains, connected to one another through NHO bridges.[47] Studies by Pauline and Corey[48] investigated polypeptide chains and proposed structures based on two hydrogen-bonded spiral configurations, with equivalent residues, except for variation in the side chain.[48] The idea that polymeric chains can adopt helical conformations was based on the latter work by Pauling & Corey who interpreted the structures of the two polypeptides namely poly-y-methyl-L-glutamate and poly-benzyl-L-glutamate determined by X-ray diffraction by Bamford, Hanby and Happey[49] in terms of the α-helix. The interpretation of the α-helix was based on the 1.5 Å reflexion (the length per residue along the axis of the α-helix) giving a 3.7 residue turn helix.[50] Perutz's earlier study[51] confirmed the 1.5 Å reflexion in hair, horn and α-keratin but he stated that that the absence of such a 1.5 Å reflexion rigorously eliminates the possibility of an α-helical arrangement for polypeptides. Pauling & Corey[52] argued that a polypeptide may have an arrangement of alpha helices packed together in such a way that the 1.5 Å reflexion would be exactly out-of-phase compared to the neighboring chain resulting in a reflexion equal to be zero. Further analysis of these crystal structures led Pauling and Corey[53] and also Crick[54, 55] to propose super helical structures. A difficulty arose in trying to explain the 5.15 Å reflexion in the k-m-

e-f proteins because a straight perfect α-helix as observed in poly- γ-methyl-L-glutamate has a 5.4 Å reflexion. To account for this apparent distortion Crick suggested that the α-helix might be deformed into a coiled-coil.[54] A coiled coil is a tertiary protein structure in which 2-7 alpha-helices are coiled together like the strands of a rope to form mainly dimeric and trimeric structures.[56] At the same time Pauling & Corey (1953) put forward a model for α-keratin based on coiled-coils. They suggested that the origin of the deformation was a repeating sequence of amino acids, a repeat every seventh residue being required for two-thirds of the α-helices in the structure, and a repeat every fourth residue for two-ninths of them.[53] In a follow-up paper Crick went on to state that the general features of the observed X-ray pattern for the k-m-e-f proteins can be predicted merely by postulating that α-helices tend to pack side-by-side in a knobs-into-holes manner and proposed two-strand rope and three-strand rope models of α-helices.[55] Clearly by 1953 the year of Watson and Crick's historical paper a lot was known about polypeptide conformations and the concept of the helix was certainly in vogue with the protein crystallographers of the day.

Early X-ray diffraction studies on DNA

Astbury and Bell published the first crystal structure of DNA in 1938, which showed that the base pairs A-T or G-C are stacked one over another and that the distance between them is equal to 3.34 Å based on X-ray studies on DNA fibers.[57] Importantly they also noted that the prominent 3.34 Å reflection is almost identical with that of a fully extended polypeptide chain system, such as β-keratin.[57, 58] In Furberg's, PhD thesis submitted in August 1949,[59] a DNA model that was a (eightfold) helix

comprising a single strand of nucleotides with stacked bases and sugar rings that displayed the conformation that he had obtained from his own X-ray crystallographic analysis of cytidine was proposed. This was no doubt also an inspiration for the Watson and Crick model although it was incorrect.[33] The cytidine structure proposed by Furberg showed D-ribose ring of cytidine to be non-planar with one of its atoms lying about 0.5 Å. from the plane containing the four remaining atoms consistent with a C3' endo configuration characteristic of A-DNA. B-DNA, on the other hand, has the C2' configuration of the ribose group. Watson and Crick based their model on Furberg's cytidine model with the C3'-endo configuration which was thus the A-DNA configuration and not the B-DNA configuration which was their aim.[33] In the Wilkins laboratory at the Wheatstone Laboratory, King's College, London, studies were undertaken on sodium thymonucleate (later known as DNA). Wilkins et al.[60] noted that DNA fibres swell and shrink markedly when the humidity was varied. By extending or drawing out DNA fibres under different humidities they observed a difference in the birefringence. In saturated water vapour the DNA fibres were mainly microscrystalline but on reducing the humidity to 50 %, a reversible change took place and the greater part of the crystallinity disappeared. They hypothesised that the extension could take place by the rotations of the bonds in the backbone-chain relative to one another but with the bond angles kept relatively constant and importantly they summized that sodium thymonucleate had a second form. The work and diffraction patterns emanating out of the Wilkins lab and analysis of Astbury and Bell's diffraction patterns was also very important in inspiring the models proposed by Watson and Crick.[33] As history shows it was Franklin's critical insight that the hydrophilic phosphate backbones of the nucleotide chains of DNA should be positioned so as to interact with water molecules on the outside of the molecule while

the hydrophobic bases should be packed into the core.[33] This was the critical piece of information that she shared with Watson and Crick at a meeting where the pair presented a somewhat embarrassing first DNA model showing the phosphates on the inside.[33] Franklin and Gosling using X-ray diffraction showed two forms of DNA as a function of humidity.[61] They coined the name structure A for the polynucleotide that occurred at about 75% relative humidity while a second structure they designated B was observed when the relative humidity increased above 75 %. From the improved diffraction patterns it was possible to predict the number of bases stacked within a single turn of the DNA helix and the symmetry. It is now known that B-DNA has 10.5-fold screwed symmetry and a pitch of 3.4 nm, while A-DNA is more compact with a pitch of 2.8 nm and a 12-fold symmetry. Of course a number of other critical pieces of information from other techniques led to the elucidation of the structure of DNA. Dekker et al. showed DNA to be a linear polymer consisting of nucleotides (sugar-base-phosphate groups), connected to each another by 3-,5-phosphodiester bonds.[62] Chargaff et al. proved that the relations of A/T and G/C are equal to one and that DNA contains a mixture of these combinations.[63] Gulland using electrochemical titration[64] concluded that the bases in DNA are connected to one another by hydrogen bonds. While X-ray crystallography can provide exquisite detail on the position of atoms for the various DNA conformations it is limited to the analysis of very pure crystals and cannot be used to monitor the dynamical conformational changes observed in solution and cells. Other techniques have also played important roles in elucidating the conformation of DNA including circular dichroism (CD), nuclear magnetic resonance (NMR), UV-Visible spectroscopy and vibrational techniques including infrared and Raman spectroscopy.

Circular Dichroism

Circular dichroism (CD) is a technique that detects the interactions of chiral molecules with circularly polarized electromagnetic rays. CD has been employed to investigate DNA using ultraviolet light within 180–300 nm range where bases of DNA absorb light.[65] The CD spectra of B-forms of synthetic polydeoxynucleotides depend on the primary sequence.[66] Most B-forms are characterized by a positive long wavelength band or bands at about 260–280 nm and a negative band around 245 nm. The precise positions and amplitudes of the CD bands depend on the base sequence and the different conformational properties.[66] The CD spectrum of A-DNA is very similar to the CD spectrum of RNA and the RNA/DNA hybrid both of which are in the A-form. The spectrum is characterized by a strong band at 260 nm and a negative band at 210 nm.[66] The CD spectrum of Z-DNA is nearly an inversion of the CD spectrum of the B-form; it contains a negative band at about 290 nm, a positive band around 260 nm and another characteristic, extremely strong negative band at 205 nm.[23] Ivanov demonstrated that the B-, A- and Z-form transitions can be very elegantly followed using CD spectroscopy.[67] CD spectroscopy has been used to study triplexes, guanine and cytosine quaduplexes, DNA fragments and DNA condensation, which have been summarised in a review article.[66]

In general DNA does not absorb light above 300 nm. Detection of signals above 300 nm indicates that the DNA is condensed into particles that scatter light and the secondary structural information is lost.[66] While CD has a number of advantages for studying DNA conformation especially for solution based studies at low concentration it can not be used to analyse DNA conformation in cells as RNA and proteins obscure the important DNA bands and light scattering from the nucleus and the whole cells can lead to scattering artefacts in the spectrum.

^{31}P NMR

High-resolution multidimensional ^{31}P NMR has provided exquisite three-dimensional structural information on duplex, hairpin loops, protein-DNA interactions and oligonucleotide structures, which are summarised in a review article.[68] NMR experiments demonstrated that the nucleic acid conformation in solution may not be identical to the static picture provided by X-ray diffraction in the crystal state.[69] By analysing the observed three-bond coupling constants with a proton-phosphorus Karplus relationship it was possible to measure the H3'-C3'-O-P torsional angle from which the C4'-C3'-O-P torsional angle could be calculated. This torsional angle proved to be very consistent for A-DNA and could be used to distinguish the A-form from the B-form.[68] NMR like CD can be applied to DNA in solution, however, it cannot be used to investigate DNA conformational change in living cells because of the myriad of contributions from other biomolecules that would obscure the important coupling constants.

FTIR spectroscopy

FTIR spectroscopy offers a number of advantages for investigating the conformation of DNA in cells, nuclei and isolated nucleic acids. 1) The technique requires no stains that could potentially interfere with the native conformation. 2) It can be applied to living cells for *in vitro* studies enabling the direct monitoring of the cell in response to environmental perturbation. 3) There are a number of distinct bands indicative of the major DNA conformations. 4) Most importantly the technique can be used to assess whether the DNA has denatured or changed its conformational form by rehydrating the sample. If upon rehydration the DNA goes into the B-form, as evidenced by the

position and intensity of the characteristic phosphodiester bands, then the DNA was in the A-form. If the phosphodiester bands remain unchanged in response to rehydration then the DNA has denatured. There are currently no other techniques that can investigate DNA conformation in functional cells and hence this is a research area where FTIR has tremendous potential.

Early infrared studies investigating DNA conformation made use of humidity controlled transmission cells. By using specific saturated salts the humidity could be controlled. The measurement of the DNA was performed between two sealed infrared transmission windows exposed to the saturated water vapour.[70] Hydration/dehydration can be performed using an Attenuated Total Reflection-Fourier Transform Infrared (ATR-FTIR) spectrometer for cells, nuclei and isolated DNA.[71] With this configuration the dry DNA, cells or nuclei can be placed on the diamond or ZnSe window of an ATR-FTIR spectrometer. Pressure is applied with a clamp directly onto the dry biological material. A drop of water or isotonic saline is placed next to the sample and allowed to gradually seep into the sample over time whilst the spectra are recorded. Alternatively, a wet sample of DNA can be placed onto the ATR crystal and spectra recorded as the DNA dries. Using this approach it was possible to record a series of spectra like those presented in Figure 5, which show the gradual hydration and dehydration of single and double stranded DNA along with RNA as a function of hydration, which will be discussed in the next section.

Single cell measurements can be performed using a synchrotron-FTIR (S-FTIR) microscope and a specially designed transmission cell that enables the water to gradually evaporate over time. One such design for a transmission cell was reported by Tobin et al.[72] who modified a ThermoFisher compression cell by replacing the windows with two CaF_2 windows. One window had a fabricated spacer with either a

single or dual outlet channel to remove excess water when the windows compressed. The spacers were fabricated by UV photolithography using a metal mask manufactured for the required size and design of spacer (MiniFAB\(Aust) Pty. Ltd., Scoresby, Australia). Two spacer patterns were designed, which are shown in Fig. 4(A) and (B). The initial design (a) incorporated a single liquid outlet but it produced strong directional capillary action resulting in loss of liquid from the cell in less than 15 min. A revised design (b) with three serpentine channels minimised that resulted in sample hold times of around 1 h. It is important to keep the path length between the windows at 6 μm or less to prevent saturation of the amide I mode by the water deformation mode at ~1644 cm^{-1}. For single cell measurements the cells are placed onto the lower window of the transmission sample holder that has the channels. The top window is clamped down onto the cells whilst looking under a stereo-microscope. The clamp is tightened until the top window is just touching the top of the cells. The transmission sample holder is then placed on the microscope stage of the FTIR microscope and spectra recorded of the cell initially hydrated. After about 30 minutes the water seeps out of the channels and the cells become dehydrated. During this process spectra are continually recorded of the same cell as it dehydrates yielding a spectral series similar to that shown in Figure 8, which will be discussed later..

Infrared spectroscopy applied to DNA conformation

Comparison of nucleic acid spectra

Vibrational approaches have found an important niche in examining the dynamics of DNA conformation. Detailed reviews on the infrared spectroscopy of nucleic acids and their bases have been undertaken by Zhizhina and Oleinik[73], M. Tsuboi[74] and Talliendier and Liquier.[3] Figure 5 compares spectra of single stranded DNA

dehydrating, single stranded RNA rehydrating, double stranded DNA dehydrating and double stranded DNA dehydrating. The spectra show a number of interesting features. For instance it is clear that single-stranded DNA shows similar shifts to double stranded DNA e.g. the ν_{asym} PO_2^- shifts from 1237 cm^{-1} to 1225 cm^{-1} in ss-DNA, while in double stranded DNA (ds-DNA) it shifts from 1239 cm^{-1} to 1227 cm^{-1}. Interestingly, the relative intensity of the ν_{sym} PO_2^- at 1087 cm^{-1} and 1054 cm^{-1} bands in single stranded DNA (ss-DNA) are much more pronounced than the corresponding bands in ds-DNA, especially when one compares the second derivative spectra (Figure 5 bottom panel). The apparent increase in the absorbance in hydrated ss-DNA may result from a type of IR hyperchromicity, which is normally observed in UV-Vis absorption spectra at 260 nm, which results from the un-stacking of the bases.[34] The molar extinction coefficient may increase upon the un-stacking of the bases giving rise to the intense phosphodiester bands observed in the infrared spectrum. There is a pronounced shift in the base pairing vibration from 1718 cm^{-1} to 1711 cm^{-1} in ds-DNA, which is not observed in ss-DNA. A band is observed at 1718 cm^{-1} in ss-DNA but it does not show the same shift as observed for ds-DNA. A small band is observed at 1691 cm^{-1} in ss-DNA, which is not observed or at least is very small in ds-DNA. Bands at 970 cm^{-1} and 936 cm^{-1} also show slight intensity increases. RNA, on the other hand, shows a slight intensity increase in the ν_{sym} PO_2^- as it becomes hydrated. The ν_{asym} PO_2^- mode at 1241 cm^{-1} does not shift in RNA as it is permanently in the A-form irrespective of hydration. There is no change in the band at 1718 cm^{-1} upon rehydration but there is a dramatic decrease in the 1690 cm^{-1} as the RNA is hydrated which is assigned to an in-plane double-bond stretching vibration of the base residues. Other unique RNA bands include those at 1217, 1177, 1120, 995 and 965 cm^{-1}. Table 2 depicts the major bands found in cells and tissues along with the important DNA

conformational band positions and assignments based on the literature. It is important to note that exact positions depend on base composition that will vary from organism to organism.

The assignment of DNA and RNA conformational marker bands

The first infrared studies on nucleic acids were performed by Blout and Fields using a Perkin-Elmer infrared spectrometer, model 12A, with a ten cycle chopper, a Strong bolometer, an alternating current amplifier, and a Brown Instrument Company recording potentiometer.[75] They were able to differentiate deoxyribonucleic acid from ribonucleic acid by their absorptions below 1100 cm^{-1} and examined spectra of nulcleotides and nucleosides.[76] They assigned absorptions in the 1750-1600 cm^{-1} to the in-plane vibrations of the base residues involving several complicated vibrations from the stretching motions of the C=N, C=O and C=C bonds from nucleic bases. Interestingly they postulated that the technique might be extended to the study nucleoproteins, nucleic acids and their degradation products extracted from normal and neoplastic tissue pointing the way forward to infrared spectroscopy in disease diagnosis. Blout and Lenormant[77] noted that the strong absorption bands at 1680 and 1645 cm^{-1} were shifted to 1660 and I625 cm^{-1} by the action of: 1) deoxyribonuclease, 2) by heating the solution for a few minutes at lOO°C, or 3) by raising the pH over 9. After performing these treatments the bands did not shift back to their original positions indicating denaturation of the double helical structure. The two strands of DNA come apart readily on incubation at pH > 12 or pH < 2 due to ionization of the bases.[34] The shell of hydration surrounding the DNA is disrupted at very high or low pH resulting in destabilizing of base stacking. Strong acid treatment of DNA results in depyrimidation and depurination and the loss of bases by cleavage of the glycosidic

bond.[34] Fraser et al.[78] performed the first infrared dichroic measurements on orientated DNA prepared from calf-thymus. They found bands at 3335, 3210, 1700, 1660, 1087, 1052 and 967 cm^{-1} were all reversed to parallel, whereas the 1235 cm^{-1} remained unchanged. These results supported Wilkins et al.[60] hypothesis that a reversible change occurs in the structure of orientated films and fibres when they are stretched or rolled. A land mark paper by Sutherland and Tsuboi investigated the NaDNA as a function of humidity.[70] Spectra were obtained from NaDNA films at different relative humidity of 0, 14, 20, 32, 52, 60, 75, 80, 90, 92 and 100 %. They noted a number of distinct changes in the spectra as the humidity increased, which included an increase in intensity of a number of bands and a shift of the band at 1240 cm^{-1} to ~1220 cm^{-1}, which they assigned to the PO_2^- antisymmetric stretching vibration based on comparison with spectra of the phosphite and the hypophosphite anion.[79] The shift of the band from 1220 to 1240 cm^{-1} in pure DNA is attributed to the removal of the water molecules, so that the PO_2^- group becomes free of any hydrogen bonding.[74] They correlated their results with the modified Watson & Crick structure for DNA based on the work of Feughelman et al.[80] but were unable to demonstrate the existence of the two crystalline forms namely A-DNA and B-DNA, which occur at low (below 75%) and high humidity (above 75 %), respectively because according to Bradbury et al.[10] they did not use a reflecting microscope to observed the more highly ordered regions, which sometimes occur only over small areas of film. Bradbury et al.[10] verified the two crystalline forms by plotting the relative humidity as a function of the dichroic ratio for the 1672 cm^{-1} band in the deuterated NaDNA film where they observed two plateaus, one for humidity's greater than 90 % r.h. and another for humidity's between 70 and 80 % r.h., which they argued corresponded to the two crystalline forms identified by Franklin and Gosling as the *A*-form at 75% r.h. and the

B-form at 92% r.h.[4] Bradbury[10] also noted that at high humidity the bands in the region 750 to 1200 cm^{-1} are sharper and better defined. They proposed that the crystallinity of the specimen improved with water uptake.

Bradbury et al.[10] also investigated lithium DNA as a function of humidity and found the B-form exists greater than 66% r.h. and a second form, different from the A-form of NaDNA originally identified by X-ray diffraction and named C-DNA[81, 82] exists between 44 and 56% r.h. where the bases are tilted by about 4 degrees from the perpendicular. The small size of the lithium ion compared to the Na counter ion provided higher quality X-ray diffraction patterns. Besides fundamental studies on the hydration of DNA, Bradbury et al.[83, 84] also investigated nucleoprotamine[83] and nucleohistone[84] as a function of humidity. Nucleoprotein is a simple basic protein found in the sperm heads of some somatic cells. They observed that the amide I and amide II modes appeared at approximately 1660 and 1550 cm^{-1}, respectively, in nucleoprotamine from protamine along with bands at 1709, 1493, 1454, 1423, 1325, 1230, 1089, 1053, 1019, 969, 895 cm^{-1} assigned to DNA component in high humidity.[83] The 1709 cm^{-1} band, which is found slightly shifted in NaDNA to 1705 cm^{-1}, is considered to be caused by the pairing of base moieties namely guanine with cytosine and adenine with thymine based on the fact it is missing in single-stranded f 1-phage DNA and is also absent in DNAase treated double-helical DNA.[85] The 1705 cm^{-1} disappears upon drying or denaturing NaDNA indicating that the hydration is needed for base pairing to take place.[85] The disappearance of this band was explained as being due to the breakdown of specific hydrogen bonds between base residues in denatured DNA.[86] In most eukaryotic cells DNA is found in combination with histones. Studies by Bradbury et al.[84] on nucleohistone showed the amide I and II modes occurring at 1660 cm^{-1} and 1545 cm^{-1}, respectively. The 1709 cm^{-1} appears as

a strong shoulder on the amide I mode and shows high perpendicular dichroism and disappears upon deuteration. The strong asymmetric phosphodiester stretching vibration at ~1230 cm^{-1} split into two components a parallel (1226 cm^{-1}) and perpendicular (1229 cm^{-1}), which upon drying shifted to 1246 cm^{-1} and 1247 cm^{-1}, respectively. Other bands were found at 1089, 1053, 1019, 972 cm^{-1} and weak bands at 937 and 894 cm^{-1}. Upon drying the bands at 1089 and 1053 cm^{-1} shifted to 1101 cm^{-1} and 1068 cm^{-1} and the definition of the spectral region between 1200-900 cm^{-1} was lost.[84] Bradbury et al.[83] demonstrated that there is a component in nulceohistone that takes more than three weeks to deuterate with D_2O vapour at 94% r.h. while in nulcleoprotein it takes only minutes. This was explained by nucleoprotein not having an α-helical structure whereas nucleohistone has an α-helix.[74] Falk et al.[87] also performed humidity studies on DNA and based on wavenumber and intensity changes concluded that the $PO_2^- Na^+$ groups of DNA become hydrated in the range of 0 to 65% relative humidity, while the hydration of the bases begins above this range. From their studies they concluded that DNA is stable in the B-DNA conformation above 75% humidity and at lower humidity a reversible transition occurs producing a disordered form where the bases are no longer stacked one above the other nor are they perpendicular to the helical axis. Falk et al.[87] hypothesized that water is first absorbed by the PO_2^- groups, followed by the C–O–P and C–O–C groups of the phosphodiester linkage with the last sites of hydration being the DNA bases. Changes observed upon dehydration were found to be similar to those which occur when DNA is denatured in solution by heating,[86] or by treatment with deoxyribonuclease,[86] or formamide.[88] Tsuboi et al.[86] noted shifts in many bands upon denaturation with deoxynuclease (37°C for 10 minutes at 75% r.h.) and which included: 1) the disappearance of the 1710 cm^{-1} and a weaker band appearing at 1690 cm^{-1}, 2) slight

weakening and shifting of the 1220 cm^{-1} band to 1241 cm^{-1} and the disappearance of the splitting of this band, 3) weakening and high frequency shifting of the 1084 cm^{-1} band to 1096 cm^{-1}, 4) high frequency shifting of the 1050 cm^{-1} band to 1069 cm^{-1} assigned to a C-O stretching vibration, 5) broadening and weakening of the 965 cm^{-1} band shifting to 957 cm^{-1} assigned to a P-O stretching vibration based on its absence in nucleotide spectra.

A study by Hamilton and Cooper[5] questioned whether humidity alone was driving the A-B conformational change. They demonstrated that the change in structure from the A to B-form in NaDNA depends on the presence of salts as well as on increase of relative humidity, and that a salt-free NaDNA does not change its structure with increasing relative humidity. Pilet and Brahms[89] performed infrared linear dichroism using calf thymus and salmon sperm DNA with ~42% G + C base composition as a function of salt concentration. Their results indicated that at very low sodium chloride content i.e. 0% there is no formation of a well-defined A-form, and the denaturation occurs already at 75% r.h. instead of 65% r.h. While at higher concentrations of sodium chloride content (7% NaCI) the plateau of the B-form is more extended towards lower humidity (i.e., at about 90% r.h. instead of 95% r.h.), and the DNA denaturation begins at 65% r.h. They concluded that at both high and low salt concentrations the pure A-form could not be observed. Pilet and Brahms[89] also used infrared dichroism to show that the conformational B-A transition is favored by high G +C content. However, at low G + C content, the A-form may not always occur, but a direct change from ordered to disordered form may result indicating the base sequence is an important factor for the B - A conformational transition.[89, 90] Brahms et al.[6] also reported a new NaDNA form, which is similar to the C-form of Li DNA. This C-like form in NaDNA occurred under conditions of very low sodium chloride

content (at high r.h.), high sodium chloride content (at low r.h.), and low G + C content of the DNA (at low r.h.).[6] More detailed studies in the 900-800 cm^{-1} of the IR spectrum of DNA revealed other conformational marker bands. Brahms et al.[91] assigned the 837 cm^{-1} band to a C-O-P-O-C backbone vibration specific for B and C-forms of DNA and bands at 812 cm^{-1} and 860 cm^{-1} to the phosphodiester chain of A-form conformations.[91] These results were in complete agreement with Pohle et al.[92] studies on DNA conformation who identified another unique A-DNA band appearing at 1185 cm^{-1} tentatively assigned to a vibration of the sugar-phosphate backbone with a fairly high contribution from the sugar moiety.[92] Brown and Peticolas[93] have reported a calculation of the vibrational normal frequencies of the DNA backbone in which they refined backbone force constants to fit the observed lines of A- and B-DNA based on a simple backbone only model consisting six backbone skeletal atoms of the polynucleotide. Lu et al.[94] performed a force-constant refinement calculation for the A-DNA, B-DNA and A-DNA backbone modes based on a more complete model. This model included the backbone phosphate-group and the complete ribose ring where the hydrogen atoms were assumed to be rigidly attached in the usual dynamic group approximation. Calculated bands matched nicely with experimental band shifts observed going from B-A DNA conformation demonstrating the efficacy of their approach. They calculated a normal mode at 1187 cm^{-1} for A-DNA, 1168 cm^{-1} for A-RNA and 1160 cm^{-1} for B-DNA, respectively. All three of these bands have been assigned to stretching vibrations of the sugar-phosphate backbone.[94]

A series of very detailed studies investigating a range of DNA conformations including A-DNA, B-DNA, C-DNA, H-DNA, double stranded RNA and synthetic polynucleotides were performed by Taillandier et al. which have been summarized in a general review article.[3] They showed that at low ionic strength solutions, native

DNAs and most synthetic double-strand poly- and oligonucleotides adopt a B-form conformation, while under the same conditions double-stranded RNAs adopt an A-type conformation.[3] They observed the base pairing vibration at 1705 cm^{-1} in the A-form, 1715 cm^{-1} in the B-form and 1695 cm^{-1} in the Z-form. Taillandier et al.[3] also noted that some DNA sequences do not undergo the B-A transition. For example, the A-form is not observed by decreasing the water content of a poly(dA), poly(dT) sample but polymer poly[d(A-T)] readily adopts this conformation. They also demonstrated that a number of polynucleotide sequences are able to adopt a Z conformation, which included alternating purine-pyrimidine sequences, poly[d(A-C).poly[d(G-T)] and poly[d(A-T)]; and AT base pairs, d(C2amino-ACGTG), d(m^5SCGCAm^5SCGTGCG) and d(mSCGTAmsCG); also sequences containing GC base pairs out of regular purine-pyrimidine alternation, d(msCGGCmsCG), d(CBr8GGCBr8G), and d(CGCGC~). FTIR spectra of Z-DNA from Taillandier's[3] work show the position of the asymmetric PO_2^- stretch appearing between 1212-1215 cm^{-1}, depending on the base-composition, which is red-shifted from both B-DNA (~1225 cm^{-1}) and A-DNA (~1240 cm^{-1}). Another distinct band indicative of Z-DNA appears at 1065 cm^{-1} from the deoxyribose moiety and there is an unassigned band between 1018-1014 cm^{-1}.[3] Liquier et al. [95] proposed a simple method to evaluate the amount of A or B forms of DNA in DNA/histone mixtures when both A- and B-forms are present. They also demonstrated that the about four to three turns of DNA helix represent the "critical length of DNA" for the B-A transition to occur. These highly controlled infrared studies using specific sequence nucleic base pairs lay a strong foundation for understanding the molecular basis of DNA conformational change.

Besides humidity,[4, 70] salt content,[5, 23] counter ion influence,[96] pH[77] and base composition[3] there are a number of other factors that can affect DNA conformation.

These include DNA intercalation, transcription and radiation damage. Transcriptional processes in cells do not result in an *en masse* change in DNA conformation and hence such small changes are unlikely to be detected in cells using conventional FTIR spectroscopy. The intercalation of drugs with DNA can cause local perturbations in the DNA helical structure depending on the type of drug and mode of intercalation.[97] The majority of intercalating agents are planar/aromatic molecules and include doxorubicin, ethidium bromide, daunomycin and acridines.[97] Such drugs are thought to inhibit both transcription and DNA replication, causing toxicity and mutations and changes in DNA conformation.

Sulforaphane, which is an isothiocyanate found in cruciferous vegetables with anti-cancer properties, resulted in a B- to A-DNA transition, while RNA remained in the A-form.[98] On the other hand the interaction of the drugs mitoxantrone[99] and curcumin[100] with DNA were shown not to cause any change in the conformation. The structural effects of lomustine on DNA were investigated using different spectroscopic approaches including ATR-FTIR and confirm the formation of an intermediate stage of DNA that occurs during the transition of B-form into the A-form.[101] Jangir et al.[102] showed that carboplatin binds to DNA through direct interaction of platin-DNA bases (guanine, thymine, adenine and cytosine), with a small perturbation of phosphate group of DNA backbone, while DNA remains in the B-conformation. DNA aggregation was also observed at higher drug concentrations.

Clearly different drugs have significantly different effects on the DNA conformation depending on the mode of action. FTIR studies investigating the interaction of DNA incubated with drugs are relatively easy to control. The same cannot be said for studying drug interactions at the functional cell level because of the intrinsic biological variability and difficulties in controlling the timing and synchronization of

the experiments. Mignolet et al.[97] provide an in-depth review on the application of FTIR spectroscopy for monitoring the effect of anti-cancer drugs on cells and tissues. It is interesting to note that the majority of studies investigating drug intercalation have been preformed on fixed cells or tissues hence the DNA is always predominantly in the A-form. It is clear from these studies that the effect of intercalating agents on DNA and cells can have a variety of effects depending on the type of drug and mode of interaction with DNA. More work is required on functional cells to establish whether DNA conformational change can be detected following incubation with intercalating agents. Such studies can be performed at the single cell level using synchrotron FTIR.[103] However, during the time taken to record the measurements on a population of inoculated cells (30-60 minutes), the control cells can change. It is also necessary to compare cells at different stages of the cell cycle in response to the therapeutic agent hence the cultures need to be synchronized. The intrinsic biological variability in the cell cycle and the difficulty recording live cells under so called "physiological" conditions necessitates the experiments be performed in triplicate and a multivariate approach applied to analyse the data.

Changes in DNA conformation can also result from exposure to various types of radiation. FTIR studies have been performed on cells following exposure to ultra-violet[103-106] and proton irradiation.[107, 108] Gault et al.[109] dosed lymphocytes by gamma arays[110, 111] and 2 Gy alpha particles[112] and analysed the cells using molecular spectroscopic techniques and reported conformational changes in the DNA. Synchrotron Radiation Fourier Transform Infrared (SR-FTIR) spectra of single human prostate adenocarcinoma PC-3 cells, irradiated with 2 MeV protons generated by a proton microbeam were compared with non-irradiated control cells. The results show a dose dependent shift of the O-P-O asymmetric stretching mode from

1234 cm^{-1} to 1237 cm^{-1}, consistent with local disorder in the B-DNA conformation along with a change in intensity of the O-P-O symmetric stretching band at 1083 cm^{-1} indicative of chromatin fragmentation.[108] SR-FTIR was used to investigate macromolecular changes in melanocytes after Ultraviolet Radiation (UVR) exposure. DNA conformational changes were observed in cells exposed to an artificial UVR solar-simulator source. These included a shift in the DNA asymmetric phosphodiester vibration from 1236 cm^{-1} to 1242 cm^{-1} in exposed cells and from 1225 cm^{-1} to 1242 cm^{-1} for irradiated nuclei indicative of a B to A-form conformational change.[103] It is important to note that for the studies mentioned above it would be difficult to distinguish the A-form from denatured DNA without performing rehydration experiments. The concept of using rehydration as an FTIR assay to determine whether DNA is simply in the A-DNA conformation or has denatured needs further exploration and is the subject of ongoing studies.

Infrared studies on RNA

When interpreting FTIR spectra of cells the contribution of RNA to spectrum can be significant[113] and often difficult to distinguish from DNA especially when the cells or tissue sections are fixed or dried and the DNA is in the A-form. Benedetti et al.[113] noted that the addition of small amounts of RNA (1±5%) to a DNA/Protein/RNA mixture modified the band shape significantly. Hence it is important to be able to differentiate RNA from A-DNA when interpreting spectra of cells and tissues.

RNA often exists in a double-helical form in transfer RNAs, ribosomal RNAs and sections of messenger RNAs where it forms an A-like helix.[34] The ribose configuration for double stranded RNA is C3' endo, which is a characteristic feature of the A-DNA helix.[34] RNA does not show the same dynamical dependence on hydration as DNA because it exists only in the A-form. The hydroxyl group attached

to the carbon of the ribose ring prevents RNA from transforming to the B-form by making it energetically unfavorable. Furthermore, RNA is chemically less stable than DNA because the C2'–OH group is easily degraded by enzymes such as ribonucleases.[35] Susi and Ard[114] recorded laser-Raman spectra and IR spectra of polycrystalline uracil, N,N-dideuterouracil, C,C-dideutero uracil, and perdeutero uracil and assigned IR absorption bands and Raman lines to fundamental modes by a comparison of the spectra of four isotopically substituted analogs. They performed a normal coordinate calculation and assigned the important normal planar modes. However, these modes appear very weak in the IR spectrum of RNA and are usually obscured by other bases, ribose and phosphodiester stretches. This is totally different to hydrated B-DNA, which has sharper and better defined bands in the 1100-700 cm^{-1} region, and hence the spectral profile of RNA is more similar to A-DNA. The spectral features are very different in NaRNA and NaDNA in the spectral region below 1100 cm^{-1}.[70] The appearance of bands near 800 and 860 cm^{-1} are observed in both deuterated and undeuterated NaRNA.[70] A band observed at 1690 cm^{-1} in NaRNA was assigned to an in-plane double-bond stretching vibration of the base residues in the RNA structure,[74] and the dichroic ratio of that band reflects the base-plane inclination, which was estimated to be 5-15 degrees on the basis of the X-ray analysis.[115] A band appearing at 1120 cm^{-1} in RNA has been assigned to a stretching vibration of a skeletal structure around the 2'-OH group of the ribose residue.[116] Calculations by Lu et al.[94] did not explicitly report a band at 1120 cm^{-1} nor was there one experimentally observed. The nearest experimental band was observed at 1101 cm^{-1} and calculated at 1107 cm^{-1} and assigned to a symmetric PO_2^- mode. However, other bands assigned to ribose-phosphate modes observed experimentally matched very well with theory 1160(1168), 977(957), 917 (890), 869(832) cm^{-1}. Ribose only bands were observed

at 1132 cm^{-1} and 1000 cm^{-1} and calculated at 1159 cm^{-1} 1014, respectively and the C-O stretch at 1049(1052) cm^{-1}. Pevsner and Diem[117] investigated RNA and DNA as a function of hydration using KBr pellets. Their results were identical to previous studies investigating conformational changes in DNA and the lack of conformational change in RNA. Studies by Wood et al.[118, 119] monitored the molecular dynamics of lymphocyte activation with FTIR microscopy. FTIR spectra of fixed lymphocytes exposed to the mitogen phytohemaglutanin were compared with control lymphocytes over time. In the first 4 hours following mitogenic activation there was a notable increase in the intensity of the PO_2^- antisymmetric stretching vibration at 1244 cm^{-1} along with a concomitant increase in bands at 1120 cm^{-1} and 1160 cm^{-1} from the C-O stretching vibrations of the ribose group. The changes are consistent with an increase in RNA synthesis, which is known to occur in the first few hours following mitogenic stimulation of lymphocytes. Hence both the 1120 cm^{-1} and 1160 cm^{-1} in combination with an increase in the intensity of the PO_2^- antisymmetric stretching vibration at 1244 cm^{-1} can be used as indicators for an increase in RNA synthesis.

DNA bands as IR markers for cancer detection

It is clear infrared spectroscopy has played a pivotal role in understanding the conformational dynamics of DNA in polynucloetides, orientated DNA films, nucleoprotein and nulcleohistone. The important bands associated with the main DNA conformations and how they change upon hydration, salt concentration, pH, deuteration, base composition, temperature and enzymatic activity had been fully elucidated. The scene was set for taking the technology into the clinic and utilizing the knowledge gained from these fundamental studies on DNA to diagnose abnormalities in cells and tissues. The premise was simple and elucidated by Henry

Mantsch one of the fathers in the field of biospectroscopy: *Furthermore, changes in tissue biochemistry must precede any morphological or symptomatic manifestations, thus allowing spectroscopic diagnosis at an earlier stage of the disease.*[120] It was so reasoned, that because cancer cells proliferate at a greater rate and have more cells undergoing mitotic division, with double their normal complement of DNA at the M2 phase of the cell cycle, then such changes must manifest in the spectra of cancerous cells when compared to their normal counter parts. While in theory this made perfect sense, in practice the detection of DNA in fixed cells became very difficult with mid-IR, because of overlapping bands and the effects of differential hydration and DNA conformation. A number of detailed reviews on the application of infrared spectroscopy to cancer diagnostics have recently been published.[121-123] The majority of FTIR studies investigating the application of FTIR to cancer diagnosis have focused on measurements performed on fixed cells where the DNA in predominantly in the A-form and therefore the DNA bands are weaker and less defined.

One of the first FTIR studies undertaken on cancerous and non-cancerous cells were reported by Benedetti et al. investigating the application of FTIR spectroscopy to leukemia diagnosis.[124] In this study they reported absorptions at 965 cm^{-1} and 530 cm^{-1} in leukaemic cells, which were absent in normal cells.[124] In a follow up paper the ratio of the integrated areas of the bands at 1080 cm^{-1} ($\nu_{symm}\, PO_2^-$) and 1540 cm^{-1} (amide II) above 1.5 were diagnostic of leukemic lymphocytes.[125] Wong and Rigas applied FTIR to a range of cancers including colorectal, colon, cervical, basal and colon adenocarcinoma cell lines. In all cases changes in phosphodiester bands were regarded as one of the important infrared markers for neoplasia and the nucleic acids were the major contributors to the spectrum of neoplastic cells.[126] However, in these early studies the biological systems were poorly understood from an infrared

perspective. Later studies identified potential confounding variables that could obscure diagnosis, especially in the case of cervical cancer, where lymphocytes and blood components became confounding varaibles.[127,128] Other studies investigated cell maturation and differentiation[129,130] demonstrating dramatic changes as cells progressed through different stages of the cell cycle as will be discussed. It was beginning to become obvious that an intrinsic understanding of the biology of the system was vitally important when diagnosing cancer using FTIR spectroscopy. A study by Wood et al.[131] applied Principal Component Analysis (PCA) to FTIR spectra of exfoliated cells collected from 276 patients. The PCA scores plot showed an excellent demarcation of normal from abnormally diagnosed samples based on a comparison histological analysis of biopsies. However, the critical PCA loading plots showed the separation was based more on strong contributions from glycogen in the normal cells and strong contributions from bands at 1544, 1400 and 1244 cm^{-1} namely the amide II, carboxylate group and amide III from proteins in abnormal cells, respectively. The 1244 cm^{-1} could also be assigned to the ($\nu_{asym} PO_2^-$), however, it was strongly correlated with the protein bands and not the ($\nu_{symm} PO_2^-$) at 1080 cm^{-1}. A combination of FTIR mapping and Unsupervised Hierarchical Cluster Analysis (UHCA) was performed on cervical tissue (86 tissue sections from 10 patients) with varying degrees of dysplasia. The results clearly demonstrated the potential to detect low-grade cervical lesions using the UHCA.[132] However, the best demarcation of cancer versus non-cancerous regions came from performing the UHCA in the amide I and II region (1700-1500 cm^{-1}) and not the phosphodiester region (1300-900 cm^{-1}). A study by Jackson et al.[133] highlighted the care that must be taken when interpreting the 1300-1200 cm^{-1} region in cells and tissues in relation to nucleic acids as contributions from collagen can also dominate this region. Diem et al.[134] observed that human cells

exhibit spectral behavior that appears to contradict the Beer-Lambert law. They reported the DNA signals in pyknotic nuclei couldn't be observed. Pyknosis is the shrinkage of inactive nuclei due to increased condensation of DNA. Diem et al.[135] noted that terminally differentiated and metabolically inactive cells, often show no DNA signals in the nucleus at all. This was first observed for superficial ectocervical cells and verified for oral mucosa cells. On the other hand, certain cells exhibited atypical spectra throughout cell division showing in general higher absorbance of the DNA bands. Diem et al.[136] concluded that the nucleosomes of an inactive nucleus would appear as "black" (i.e., opaque or nearly opaque) strings or dots that yield no spectral information from the DNA. They hypothesised that large DNA signals observed during cell division, could be caused by transcription or replication, where the dense packing of DNA is abandoned, and the DNA becomes "visible" or detectable, in the infrared spectra, which came to be known as the dark DNA hypothesis.[134] They did emphasize that they considered this still a hypothesis that requires further experimental verification.[136] Our group performed a pivotal experiment comparing the FTIR spectrum of human anucleated erythrocytes with avian nucleated erythrocytes and also confirmed the lack of the DNA bands in the spectra of nucleated cells and published a joint paper with the Diem group on the subject.[136] Figure 6 shows the spectra recorded of the human and avian erythrocytes, which clearly shows the spectra almost identical in the phosphodiester region (1300-900 cm^{-1}). However, when the nuclei were extracted the DNA bands appeared enhanced.[136] So there was a conundrum as to why the DNA bands virtually disappeared when recording FTIR spectra of cells and tissues after fixation/dehydration and the answer lay in the change in DNA conformation that occurs upon dehydration. Moreover, this has important implications in using

phosphodiester bands as indicators for cancer detection.

It should be noted that genetic instabilities are thought to be involved in the aetiology of many cancers.[137] Genetic instabilities can result from replication, recombination, repair, and transcription and are a form of mutagenesis resulting in non-B-conformations.[7] These mutations usually occur where there are large abundance of repeat sequences[7] but would not cause on *en masse* change in the DNA conformation and therefore would be difficult to detect with conventional FTIR.

The effect of hydration and dehydration on the FTIR spectra of cells

During a visit to the Australian Synchrotron I noticed members of Dr Carolyn Dillon's group (University of Wollongong) performing some measurements on live lymphocytes. I was immediately surprised by the intensity of the phosphodiester bands in the spectra of the live cells compared to earlier studies by Wood et al. on fixed activated and non-activated lymphocytes.[118, 119] I subsequently performed some basic ATR experiments on hydrated and dehydrated avian erythrocytes and to my surprise the DNA bands appeared and disappeared, as the cells were hydrated-dehydrated-rehydrated. The results were presented at the FTIR workshop in Berlin.[138] After the workshop myself along with Dr Peter Lasch and Dr Heinz Fabian (Robert Koch Institute, Berlin) performed some experiments where we gradually hydrated avian erythrocytes with water vapour using a purpose-built sample holder developed in Professor Dieter Naumann's laboratory. The spectra from that experiment are presented in Figure 7 and show the dramatic enhancement of the $\nu_{sym}\,PO_2^-$ at 1080 cm^{-1} and the band at 1052 cm^{-1} from the C-O stretch of the ribose group. A shift from 1240 cm^{-1} to 1220 cm^{-1} was also observed and the band at 1708 cm^{-1} shifted to 1715

cm^{-1} as the cells became gradually hydrated. My Honours student at the time, Dr Donna Whelan, made the important DNA conformational assignments by comparing the band positions in the spectra of hydrated and dehydrated cells with the earlier literature on DNA conformation.[71] Figure 8 depicts the S-FTIR transmission spectra of lymphocytes as they are rehydrated. Once again there is a clear shift in the ν_{sym} PO_2^- from 1222 to 1238 cm^{-1}. The band at 1644 cm^{-1} is assigned to the H_2O bending mode, which naturally increases as the cells are rehydrated. The band at ~1650 cm^{-1} and ~1544 cm^{-1} assigned to the amide I and II modes, respectively, also increase as a function of moisture uptake. Other bands that increase in intensity include the ν_{sym} PO_2^- at 1087 cm^{-1} and the C-O stretching vibration at 1050 cm^{-1}. The band at 965 cm^{-1} shifts to 970 cm^{-1} and the base pairing vibration at 1713 cm^{-1} undergoes an intensity increase and a small shift upon rehydration to 1715 cm^{-1}. Rodent fibroblasts also showed the same general pattern upon rehydration indicating the response appears ubiquitous in all eukaryotic cells.[139] In all cases, the cells could be hydrated-dehydrated-rehydrated showing the same general changes in the DNA, indicating the conformational change occurs irrespective of the DNA in the cell nucleus. Cells fixed in ethanol can also undergo the same conformational change, however, formalin fixed DNA cannot undergo the reversible conformational change. The critical finding from these experiments is that the DNA is not invisible to infrared light in fixed or dehydrated cells but rather it adopts the A-DNA conformation and hence the bands appear weaker, broader and more diffuse and tend to be overlapped by other protein and carbohydrate bands. The B-DNA to A-DNA conformation that was so well documented in the past had somehow been overlooked when interpreting the spectra of dehydrated fixed cells. Hence the “dark DNA” hypothesis can now be dismissed and the lack of DNA observed in fixed/dehydrated cells explained as the result of the

DNA adopting the more disordered A-DNA conformation. Moreover, the DNA can be quantified in single hydrated and dehydrated cells. This is only the case for simple cells where there are not too many bands overlapping the important DNA bands.[140] The increase in intensity of the bands observed in the extracted nucleus, as mentioned above, could be explained by the fact that all of the water had not been removed prior to recording the FTIR spectra and hence the bands appeared more intense compared to the spectra of the whole avian cells. This highlights the care that must be taken when interpreting changes based on the intensity of the phosphodiester bands as small changes in the relative humidity can lead to large changes in the intensity of the important DNA bands. This is especially pertinent for cells fixed by non-crosslinking fixatives such as ethanol/methanol or though simple air-drying.

Quantification of DNA in fixed cells using FTIR spectroscopy

In a follow up study the ability of FTIR to quantify DNA in a simple eukaryotic cell (avian erythrocyte) was investigated.[140] To this end a calibration set was established using a mixture of haemoglobin and DNA and the ratio calculated based on the integrated area underneath either the $\nu_{sym}\,PO_2^-$ or $\nu_{asym}\,PO_2^-$ over the integrated area of the amide II mode or alternatively using just the direct absorbance values. The regression coefficients for the calibration were ~ 0.90 irrespective of whether the mixtures were hydrated or dehydrated. Using this simple calibration standard it was possible to predict the approximate percentage of DNA in an avian erythrocyte to an excellent degree of accuracy for both the hydrated and dehydrated cells. The amount of nucleic acids in avian erythrocytes is ~ 12.5%, with protein in the form of hemoglobin 72%, and histone 13%, with small contributions from other biomolecules such as carbohydrates and lipids.[141, 142] In the analysis of the intact erythrocytes

(~12.5% DNA), the best estimates were achieved using hydrated spectra for both the regression model and the test cell spectra (12.8 ± 4.3%). The prediction of nucleic acids in the dehydrated cell spectra using the hydrated spectra regression model underestimated the nucleic acid content (9.9 ± 4.2%), which is still in good agreement with the 12.5 % determined from earlier studies,[141] especially when taking into account the different states of hydration for the calibration and test set. Estimates for nucleic acid content of nuclei were also very good with hydrated sample spectra matched to a hydrated spectra regression model giving a prediction of 44.2 ± 6.6% nucleic acids.[140] A multivariate calibration model was developed using Partial Least Squares Regression (PLS-R) over the entire fingerprint region, which showed very similar results to the univariate analysis.[140] The conclusion from this study is that the Beer-Lambert's Law is obeyed and can be used to predict the amount of DNA in cells dismissing previous claims of non-Beer-Lambert behavior.[134,136] The avian erythrocyte is a model system for such quantification as it is essentially a bag of hemoglobin with a nucleus. In more complex eukaryotic cells like fibroblasts or ectocervical cells one could not expect to achieve the same prediction capability because of overlapping bands from collagen and glycogen, respectively. However, this is not the result of the DNA becoming too dense or opaque but rather stronger contributions from other bands obscuring the DNA bands. The apparent lack of DNA signal in dehydrated cells is simply the result of the DNA conformation changing from B-DNA to A-DNA causing a decrease in intensity of some bands and a broadening of the spectral features. This had been well and truly documented in the late 1950s[70] and early 1960s[10] but somehow forgotten when it came to interpreting spectra of dehydrated cells and tissues.

Synchrotron FTIR of live cells progressing through the cell cycle

Cell cycle heterogeneity can be a potential confounding variable in the FTIR diagnosis of cancer at the single cell.[143] A number of studies have attempted to analyse spectral changes related to cell phase using both FTIR and Raman spectroscopy.[139, 143-150] Many of these studies focused on investigating dehydrated cells and thus have lacked the ability to detect significant contributions from the DNA. Hollman et al.[147] were the first to apply synchrotron FTIR to living cells *in vitro* at different points in the cell cycle. Clear changes were observed in the spectral regions corresponding to proteins, DNA, and RNA as the cell progressed from the G(1)-phase to the S-phase and finally into mitosis. Theses included secondary structural changes in cellular proteins, along with changes in DNA/RNA content and packing as the cell cycle progressed. No changes in DNA conformation were reported. Boydston-White et al.[151] recorded FTIR spectra of HeLa cells fixed at the S-phase and the G1/G2 phase of the cell cycle. The differences observed at the various time points of the cell cycle manifested mainly as changes of the amide I and II bands, and to a lesser extent, the DNA bands regions at 1090 and 1235 cm^{-1}.[151] S-phase spectra did not form a distinct cluster on a PC3/PC2 scores plot and had much larger variance compared to the G1/G2 cells. They concluded that the heterogeneity of the S-phase spectra is large, and S-phase spectra cannot easily be separated from G1 and G2 phase spectra based on the amide I/II band profiles.[151] Bedolla et al.[144] report on the use of FTIR microspectroscopy in combination a with microfluidic device as an alternative technique for studying cell cycle distribution in live cells. By applying hierarchical cluster analysis to spectra in the 1300-1000 cm^{-1} region clusters of cells were observed which correlated well with flow cytometry results for G_0/G_1, S and G_2/M phases. Recently Fale et al.[152] investigated PC3 and HeLa cells inoculated with 1 μM

and 0.1 μM doxorubicin, respectively, showed a decrease in the nucleic acid region while an increase was observed in the protein regions. Possible explanations for the observed decrease in nucleic acid bands include that there is a change in conformation of the DNA with the presence of drug or the cell entered a different phase of the cell cycle. However, the results demonstrated that the phosphodiester bands did not change in the control sample demonstrating that the cell cycle did not contribute to the change. This was possibly the result of the cells not been synchronised and therefore the effect of the different phases of the cell cycle were averaged and not shown.[152] Whelan et al.[139] applied synchrotron FTIR spectroscopy to investigate the post-mitotic cell cycle on live cells. During exponential growth cells are constantly dividing or preparing to divide in comparison to the quiescent phase (G_0) observed in normal functioning cells prior to cell division. Figure 9A shows a schematic of the post mitotic cell cycle and the time points where spectra were collected during the cell cycle.[139] Figure 9B shows averaged vector normalized spectra from 3 trials between 11 and 21 hours showing dramatic differences in the CH stretching (3100-2800 cm^{-1}) and the phosphodiester (1300-1000 cm^{-1}). Figure 9C shows PCA scores plot (PC1 versus PC2) showing spectra collected of cells from 3 different cultures but at the same time points. The clustering of the M+1 and M+3 time points demonstrates the reproducible and consistent differences that can be achieved using live cells. During the first ten hours post mitosis, cells are observed to increase in protein and decrease in both lipid and nucleic acid concentration. During the synthesis phase, (beginning 9–11 hours post-mitosis) the PCA Loadings Plots show the accumulation of lipids within the cell as well the duplication of the genome as evidenced by strong DNA contributions.[139] In the 4–6 hours following the synthesis phase, the cells once again accumulate protein while the relative nucleic acid and lipid concentrations decrease.

Here, it was observed that during the G1 and G2 phases, the relative intensity of nucleic acid and lipid absorptions decreased while protein was synthesized, whereas during the S phase, the relative intensity of protein absorptions decreased as the nucleic acid relative concentration increased slightly and the lipid concentration increased dramatically.[139] These results are contrary to the Boydston-White study,[145] which was performed on fixed cells, where there was a lot of heterogeneity in relation to the intensity of the phosphodiester bands, especially in the S-phase. Whelan et al.[139] demonstrated that there is a reproducible increase in the DNA bands in the S-phase and the results were consistent with what is expected to biochemically change during the post-mitotic cycle.[139] By performing FTIR analysis of cells in the hydrated state, the refractive index of the background (isotonic saline), is closely matched to the actual cell hence reducing the effects of light dispersion. Mie scattering effects, which can result from particles on the order of infrared wavelengths (25-2.5 μm) scattering infrared photons, leading to sinusoidal oscillations in the baseline,[136] are also minimised in the hydrated state. Mie scattering appears more apparent when recording FTIR measurements of fixed or air-dried cells compared to hydrated cells and requires sophisticated multivariate spectral processing algorithms to remove the baseline and correct the band positions in the spectra.[153] Moreover, because the DNA is in the B-form, the DNA bands are sharper, larger and can be used to discriminate between the different time points solely in the phosphodiester region. However, no evidence of DNA conformational change was reported as the cells progressed through the post-mitotic cell cycle.

Importance of A-DNA in the survival of bacteria after desiccation

Bacteria are known to survive for prolonged periods of desiccation. In order to determine what role the DNA conformation may play in the ability of the bacteria to survive dehydration a series of hydration, dehydration and rehydration studies were performed.[22] This transition of the cellular B- to A-DNA upon dehydration had previously only been reported once by Mohr et al.[20] who noted that SASPs in *Bacillus subtilis* promote A-B DNA conformation change such that it reaches completion with significantly less reduction in humidity than is required for the process with DNA alone. Four bacteria species namely *Proteus vulgaris, E. coli, Salmonella enterica* serovar *typhimurium* and *P. aeruginos* were dehydrated and rehydrated and their ATR spectra recorded during the process. In all cases the classic B-A-B transition was observed, which included the shift of the $\nu_{asym}PO_2^-$, intensity changes in the $\nu_{sym}PO_2^-$ and the 970 cm^{-1} band. Figure 10 shows infrared spectra of a colony of *E. coli* before and after rehydration. The spectra clearly show the important DNA conformational bands shifting from the A-form to the B-form as the cell is rehydrated. In all cases once the cells were rehydrated they were able to reproduce and produce functional progeny. A-DNA had not previously been considered the conformation of DNA prevalent during the desiccation and survival of prokaryotes. The predominantly A-form DNA observed in prokaryotes necessitates further consideration of the B–A conformational transition and its role in defense mechanisms as well as its potential evolutionary role.

Summary

The importance of hydration and DNA conformation in the interpretation of FTIR spectra of cells and tissues is of critical importance in diagnosing neoplasia. It is clear

that in the dehydrated cells the DNA adopts the A-form conformation and the bands are reduced in intensity and appear broad and are often obscured by protein and carbohydrate modes. The B-A conformational change explains the apparent loss of DNA signal in fixed or air-dried cells. This makes it difficult to diagnose cancerous cells based on the contribution of DNA to the spectrum. On the other hand, in the B-DNA conformation when the cells are hydrated, the DNA bands are much more pronounced and easily identified above the protein and other biomolecular contributions. Performing hydration/dehydration of cells and tissues enables the DNA bands to be easily assigned by simply monitoring the shifts and intensity changes. DNA can be quantified in a simple eukaryotic cell such as an avian erythrocyte both in the hydrated or dehydrated state, albeit with less error in the case of the hydrated state. Quantification in more complex cells can be more prone to error due to overlapping protein and carbohydrate bands. The high quality spectra that can be obtained from single cells in the hydrated state using a synchrotron light source enabled specific stages in the cell cycle to be identified by characteristic and reproducible changes in the DNA absorption bands. Such reproducibility and information could not be achieved using fixed cells because of scattering artifacts giving rise to large spectral heterogeneity.

The biological significance of DNA conformational change is still being unraveled but in the case of bacteria the conformational change appears on *en masse* and the bacteria can survive and produce progeny. More research is required into how the DNA conformation can be preserved in the B-form in cells and tissues in the dehydrated state, as this will improve cancer diagnosis. One alternative is a point-of-care ATR device that can be directly used to target cells and tissues in the hydrated

state thus enabling the sharper more pronounced DNA bands to be observed which will in turn improve the diagnostic capability of the FTIR technique.

Acknowledgements

BRW is supported by an Australian Research Council (ARC) Future Fellowship grant FT120100926. I acknowledge Mr Finlay Shanks for instrumental support and Dr Ewelina Lipiec for constructing Figures 1, 2 and 3. I gratefully acknowledge Mr Anthony K. Eden for proof reading the manuscript. Synchrotron beam time was awarded by the Australian Synchrotron under the merit-based proposal scheme.

References

1. D. W. Urserry, in *Encyrcloperdia of life sceicnes*, John Wiley & Sons Ltd, . Chichester, 2002.
2. V. N. Potaman and R. R. Sinden, in *Madame Curie Bioscience Database [Internet].* Landes Bioscience, Austin (TX), 2000.
3. E. Taillandier and J. Liquier, *Methods in enzymology*, 1992, **211**, 307-335.
4. R. E. Franklin and R. G. Gosling, *Acta Crystallogr*, 1953, **6**, 673-677.
5. P. J. Cooper and L. D. Hamilton, *Journal of molecular biology*, 1966, **16**, 562-&.
6. J. Brahms, J. Pilet, T. T. Phuong Lan and L. R. Hill, *Proc Natl Acad Sci U S A*, 1973, **70**, 3352-3355.
7. A. Bacolla and R. D. Wells, *Molecular carcinogenesis*, 2009, **48**, 273-285.
8. R. R. Sinden, in *DNA Structure and Function*, ed. R. R. Sinden, Academic Press, San Diego, 1994, pp. 1-57.
9. G. Burckhardt, C. Zimmer and G. Luck, *FEBS letters*, 1973, **30**, 35-39.
10. E. M. Bradbury, W. C. Price and M. H. F. Wilkinson, *J. Mol. Biol.*, 1961, **3**, 301-317.
11. A. Rich, *Proceedings of the National Academy of Sciences*, 1960, **46**, 1044-1053.
12. G. Milman, R. Langridge and M. J. Chamberlin, *Proc Natl Acad Sci U S A*, 1967, **57**, 1804-1810.
13. A. Rich, *The Journal of biological chemistry*, 2006, **281**, 7693-7696.
14. L. Fairall, S. Martin and D. Rhodes, *EMBO J*, 1989, **8**, 1809-1817.
15. L. Nekludova and C. O. Pabo, *Proc Natl Acad Sci U S A*, 1994, **91**, 6948-6952.
16. Y. Timsit, *J Biomol Struct Dyn*, 2000, **17 Suppl 1**, 169-176.
17. D. Flatters, M. Young, D. L. Beveridge and R. Lavery, *J. Biomol. Struct. Dyn.*, 1997, **14**, 757-765.

18. G. Guzikevich-Guerstein and Z. Shakked, *Nature structural biology*, 1996, **3**, 32-37.
19. A. Jacobo-Molina, J. Ding, R. G. Nanni, A. D. Clark, Jr., X. Lu, C. Tantillo, R. L. Williams, G. Kamer, A. L. Ferris, P. Clark and et al., *Proc Natl Acad Sci U S A*, 1993, **90**, 6320-6324.
20. S. C. Mohr, N. V. H. A. Sokolov, C. HE and P. Setlow, *Proc. Natl. Acad. Sci.*, 1991, **88**, 77-81.
21. F. DiMaio, X. Yu, E. Rensen, M. Krupovic, D. Prangishvili and E. H. Egelman, *Science*, 2015, **348** 914-917.
22. D. R. Whelan, T. J. Hiscox, J. I. Rood, K. R. Bambery, D. McNaughton and B. R. Wood, *Journal of the Royal Society, Interface / the Royal Society*, 2014, **11**, 20140454.
23. F. M. Pohl and T. M. Jovin, *Journal of molecular biology*, 1972, **67**, 375-396.
24. T. J. Thamann, R. C. Lord, A. H. Wang and A. Rich, *Nucleic Acids Res*, 1981, **9**, 5443-5457.
25. A. Rich and S. Zhang, *Nature reviews. Genetics*, 2003, **4**, 566-572.
26. E. M. Lafer, R. P. Valle, A. Moller, A. Nordheim, P. H. Schur, A. Rich and B. D. Stollar, *The Journal of clinical investigation*, 1983, **71**, 314-321.
27. P. Vasudevaraju, Bharathia, G. R.M., K. Sambamurti and K. S. J. Rao, *Brain Reseaech reviews* 2008, **8**, 136-148.
28. R. Treffer, R. Bohme, T. Deckert-Gaudig, K. Lau, S. Tiede, X. Lin and V. Deckert, *Biochemical Society transactions*, 2012, **40**, 609-614.
29. A. Centrone, *Annual review of analytical chemistry*, 2015, **8**, 101-126.
30. R. Treffer, X. Lin, E. Bailo, T. Deckert-Gaudig and V. Deckert, *Beilstein journal of nanotechnology*, 2011, **2**, 628-637.
31. E. Lipiec, R. Sekine, J. Bielecki, W. M. Kwiatek and B. R. Wood, *Angewandte Chemie*, 2014, **53**, 169-172.
32. L. V. Yakushevich, *Nonlinear Physics of DNA*, WILEY-VCH Verlag GmbH & Co, Weinheim, 2004.
33. S. Arnott, *Trends Biochem Sci*, 2006, **31**, 349-354.
34. R. R. Sinden, *DNA Structure and Function*, Elsevier Inc, 1994.
35. R. E. Dickerson, *Sci. Am.*, 1983, **249**, 94-110.
36. D. Rhodes and A. Klug, *Nature*, 1980, **286**, 573-578.
37. T. A. Early and D. R. Kearns, *Proc Natl Acad Sci U S A*, 1979, **76**, 4165-4169.
38. M. Levitt, *Cold Spring Harbor symposia on quantitative biology*, 1983, **47 Pt 1**, 251-262.
39. M. D. Barkley and B. H. Zimm, *J. Chem. Phys.*, 1979, **70**, 2991-3007.
40. Z.-J. Tan and S.-J. Chen, *Biophysical Journal*, 2006, **90**, 1175-1190.
41. J. D. Watson and F. H. Crick, *Nature*, 1953, **171**, 737-738.
42. J. D. Watson and F. H. Crick, *Nature*, 1953, **171**, 964-967.
43. R. O. Herzog and W. Jancke, in *Verwendung von Röntgenstrahlen zur Untersuchung metamikroskopischer biologischer Strukturen*, ed. C. Neuberg, Springer Berlin Heidelberg, Berlin, 1921, pp. 118-120.
44. K. H. Meyer and H. Mark, *Ber. Dtsch. chem. Ges.*, 1928, **61**, 1932-1936.
45. K. H. Meyer, *Bichem. Z.*, 1928, **214**, 253.
46. K. H. Meyer and H. Mark, *Nature*, 1951, **167**, 736.
47. M. L. Huggins, *Chem Rev*, 1943, **32**, 195-218.
48. L. Pauling and R. B. Corey, *J Am Chem Soc*, 1950, **72**, 5349-5349.

49. C. H. Bamford, W. E. Hanby and F. Happey, *Proceedings of the Royal Society of London. Series A, Mathematical and Physical Sciences*, 1951, **205**, 30-47.
50. L. Pauling, R. B. Corey and H. R. Branson, *P Natl Acad Sci USA*, 1951, **37**, 205-211.
51. M. F. Perutz, *Nature*, 1951, **167**, 1053-1054.
52. L. Pauling and R. B. Corey, *Nature*, 1951, **168**, 550-551.
53. L. Pauling and R. B. Corey, *Nature*, 1953, **171**, 59-61.
54. F. H. Crick, *Nature*, 1952, **170**, 882-883.
55. F. H. Crick, *Acta. Cryst.*, 1953, **6**, 689-697.
56. J. Liu, Q. Zheng, Y. Deng, C.-S. Cheng, N. R. Kallenbach and M. Lu, *Proceedings of the National Academy of Sciences*, 2006, **103**, 15457-15462.
57. W. T. Astbury and F. O. Bell, *Nature*, 1938, **140**, 747-748.
58. W. T. Astbury, *Nature*, 1937, **140**, 968-969.
59. S. Furberg, Birkbeck College, 1949.
60. M. H. F. Wilkins, R. G. Gosling and W. E. Seeds, *Nature*, 1951, **167**, 759-760.
61. R. E. Franklin and R. G. Gosling, *Nature*, 1953, **171**, 740-741.
62. C. A. Dekker, A. M. Michelson and A. R. Todd, *Journal of the Chemical Society (Resumed)*, 1953, 947-951.
63. E. Chargaff, S. Zamenhof and C. Green, *Nature*, 1950, **165**, 756-757.
64. J. M. Gulland, *Symposia of the Society for Experimental Biology*, 1947, 1-14.
65. J. Kypr and M. Vorlickova, *General physiology and biophysics*, 1986, **5**, 415-421.
66. J. Kypr, I. Kejnovska, D. Renciuk and M. Vorlickova, *Nucleic Acids Res*, 2009, **37**, 1713-1725.
67. V. I. Ivanov and E. E. Minyat, *Nucleic Acids Res*, 1981, **9**, 4783-4798.
68. D. G. Gorenstein, *Methods in enzymology*, 1992, **211**, 254-286.
69. D. G. Gorenstein, S. A. Schroeder, J. M. Fu, J. T. Metz, V. Roongta and C. R. Jones, *Biochemistry*, 1988, **27**, 7223-7237.
70. G. B. B. M. Sutherland and M. Tsuboi, *Proc R Soc Lon Ser-A*, 1957, **239**, 446-463.
71. D. R. Whelan, K. R. Bambery, P. Heraud, M. J. Tobin, M. Diem, D. McNaughton and B. R. Wood, *Nucleic Acids Res*, 2011, **39**, 5439-5448.
72. M. J. Tobin, L. Puskar, R. L. Barber, E. C. Harvey, P. Heraud, B. R. Wood, K. R. Bambery, C. T. Dillon and K. L. Munro, *Vibrational Spectroscopy*, 2010, **53**, 34-38.
73. G. P. Zhizhina and E. F. Oleinik, *Russian Chemical Reviews*, 1972, **41**, 258-280.
74. M. Tsuboi, *App. Spectrosc. Rev.*, 1969, **3**, 45-90.
75. E. R. Blout and M. Fields, *Science*, 1948, **107**, 252.
76. E. R. Blout and M. Fields, *The Journal of biological chemistry*, 1949, **178**, 335-343.
77. E. R. Blout and H. Lenormant, *Biochimica et biophysica acta*, 1954, **15**, 303.
78. M. J. Fraser and R. D. B. Fraser, *Nature*, 1951, **167**, 761-762.
79. M. Tsuboi, *J. Am. Chem. Soc.*, 1957, **79**, 1351-1354.
80. M. Feughelman, R. Langridge, W. E. Seeds, A. R. Stokes, H. R. Wilson, C. W. Hooper, M. H. Wilkins, R. K. Barclay and L. D. Hamilton, *Nature*, 1955, **175**, 834-838.
81. D. A. Marvin, M. Spencer, M. H. Wilkins and L. D. Hamilton, *Nature*, 1958, **182**, 387-388.

82. D. A. Marvin, M. Spencer, M. H. Wilkins and L. D. Hamilton, *Journal of molecular biology*, 1961, **3**, 547-565.
83. E. M. Bradbury, W. C. Price and G. R. Wilkinson, *Journal of molecular biology*, 1962, **4**, 39-49.
84. E. M. Bradbury, W. C. Price, G. R. Wilkinson and G. Zubay, *Journal of molecular biology*, 1962, **4**, 50-60.
85. F. S. Parker, *Applications of infrared spectroscopy in biochemistry, biology and medicine*, Plenum Press, New York, 1971.
86. M. Tsuboi, *Prog. Theorel. Phys. (Kyoto)*, 1961, **Supp. 17**, 99.
87. M. Falk, K. A. Hartman and R. C. Lord, *J Am Chem Soc*, 1963, **85**, 387-&.
88. Y. Kyogoku, M. Tsuboi, T. Shimanouchi and I. Watanabe, *Journal of molecular biology*, 1961, **3**, 741-745.
89. J. Pilet and J. Brahms, *Biopolymers*, 1973, **12**, 387-403.
90. J. Pilet and J. Brahms, *Nature: New biology*, 1972, **236**, 99-100.
91. S. Brahms, J. Brahms and J. Pilet, *Israel J Chem*, 1974, **12**, 153-163.
92. W. Pohle and H. Fritzsche, *Nucleic Acids Research*, 1980, **8**, 2527-2535.
93. E. B. Brown and W. L. Peticolas, *Biopolymers*, 1975, **14**, 1259-1271.
94. K. C. Lu, E. W. Prohofsky and L. L. Van Zandt, *Biopolymers*, 1977, **16**, 2491-2506.
95. J. Liquier, J. Taboury, E. Taillandier and J. Brahms, *Biochemistry*, 1977, **16**, 3262-3266.
96. R. Langridge, H. R. Wilson, C. W. Hooper and M. H. Wilkins, *J. Mol. Biol.*, 1960, **2**, 19-37.
97. A. Mignolet, A. Derenne, M. Smolina, B. R. Wood and E. Goormaghtigh, *BBA-Proteins and Proteomics*, 2015.
98. F. Abassi Joozdani, F. Yari, P. Abassi Joozdani and S. Nafisi, *PloS one*, 2015, **10**, e0127541.
99. S. Agarwal, D. K. Jangir and R. Mehrotra, *Journal of photochemistry and photobiology. B, Biology*, 2013, **120**, 177-182.
100. S. Nafisi, M. Adelzadeh, Z. Norouzi and M. N. Sarbolouki, *DNA and cell biology*, 2009, **28**, 201-208.
101. S. Agarwal, D. K. Jangir, P. Singh and R. Mehrotra, *Journal of photochemistry and photobiology. B, Biology*, 2014, **130**, 281-286.
102. D. K. Jangir, G. Tyagi, R. Mehrotra and S. Kundu, *Journal of Molecular Structure*, 2010, **969**, 126-129.
103. E. Lipiec, K. R. Bambery, P. Heraud, W. M. Kwiatek, D. McNaughton, M. J. Tobin, C. Vogel and B. R. Wood, *The Analyst*, 2014, **139**, 4200-4209.
104. D. Pozzi, P. Grimaldi, S. Gaudenzi, L. Di Giambattista, I. Silvestri, S. Morrone and A. Congiu Castellano, *Radiation research*, 2007, **168**, 698-705.
105. L. Di Giambattista, P. Grimaldi, S. Gaudenzi, D. Pozzi, M. Grandi, S. Morrone, I. Silvestri and A. Congiu Castellano, *European biophysics journal : EBJ*, 2010, **39**, 929-934.
106. S. M. Ali, F. Bonnier, K. Ptasinski, H. Lambkin, K. Flynn, F. M. Lyng and H. J. Byrne, *The Analyst*, 2013, **138**, 3946-3956.
107. E. Lipiec, K. R. Bambery, P. Heraud, C. Hirschmugl, J. Lekki, W. M. Kwiatek, M. J. Tobin, C. Vogel, D. Whelan and B. R. Wood, *Journal of Molecular Structure*, 2014, **1073**, 134-141.

108. E. Lipiec, K. R. Bambery, J. Lekki, M. J. Tobin, C. Vogel, D. R. Whelan, B. R. Wood and W. M. Kwiatek, *Radiation research*, 2015, **184**, 73-82.
109. N. Gault, J. L. Poncy and J. L. Lefaix, *Canadian journal of physiology and pharmacology*, 2004, **82**, 38-49.
110. N. Gault and J. L. Lefaix, *Radiation research*, 2003, **160**, 238-250.
111. N. Gault, O. Rigaud, J. L. Poncy and J. L. Lefaix, *International journal of radiation biology*, 2005, **81**, 767-779.
112. N. Gault, O. Rigaud, J.-L. Poncy and J.-L. Lefaix, *Radiation research*, 2007, **167**, 551-562.
113. E. Benedetti, E. Bramanti, F. Papineschi, I. Rossi and E. Benedetti, *App. Spectrosc.*, 1997, **51**, 792-297.
114. H. Susi and J. C. Ard, *Spectrochim. Acta*, 1971, **276**, 1549-1582.
115. T. Sato, Y. Kyogoku, S. Higuchi, Y. Mitsui, Y. Iitaka, M. Tsuboi and K. I. Miura, *Journal of molecular biology*, 1966, **16**, 180-190.
116. M. Tsuboi, K. Matsuo, T. Shimanouchi and Y. Kyogoku, *Spectrochim. Acta*, 1963, **19**, 1617-1618.
117. A. Pevsner and M. Diem, *Biopolymers*, 2003, **72**, 282-289.
118. B. R. Wood, B. Tait and D. McNaughton, *App. Spectrosc.*, 2000, **54**, 353-359.
119. B. R. Wood, B. Tait and D. McNaughton, *Human immunology*, 2000, **61**, 1307-1314.
120. H. H. Mantsch and M. Jackson, *J. Mol. Struct.*, 1995, **347**, 187-206.
121. G. Bellisola and C. Sorio, *American journal of cancer research*, 2012, **2**, 1-21.
122. K. Malek, B. R. Wood and K. R. Bambery, in *Optical Spectroscopy and Computational Methods in Biology and Medicine*, ed. M. Baranska, Springer, 2014, pp. 419-473.
123. D. McNaughton and B. R. Wood, in *New Approaches in Biomedical Spectroscopy*, eds. H. Kneipp and E. Wentrup-Byrne, ACS Books, USA, 2007, pp. 14-29.
124. E. Benedetti, F. Papineschi, P. Vergamini, R. Consolini and G. Spremolla, *Leukemia research*, 1984, **8**, 483-489.
125. E. Benedetti, M. P. Palatresi, P. Vergamini, F. Papineschi, M. C. Andreucci and G. Spremolla, *App. Spectrosc.*, 1986, **40**, 39-43.
126. P. T. Wong, E. D. Papavassiliou and B. Rigas, *App. Spectrosc.*, 1991, **45**, 1563-1567.
127. B. R. Wood, M. A. Quinn, B. Tait, M. Ashdown, T. Hislop, M. Romeo and D. McNaughton, *Biospectroscopy*, 1998, **4**, 75-91.
128. M. J. Romeo, B. R. Wood, M. A. Quinn and D. McNaughton, *Biopolymers*, 2003, **72**, 69-76.
129. L. Chiriboga, P. Xie, H. Yee, V. Vigorita, D. Zarou, D. Zakim and M. Diem, *Biospectroscopy*, 1998, **4**, 47-53.
130. M. J. Romeo, B. R. Wood and D. McNaughton, *Vibrational Spectroscopy*, 2002, **28**, 167-175.
131. B. R. Wood, M. A. Quinn, F. R. Burden and D. McNaughton, *Biospectroscopy*, 1996, **2**, 143-153.
132. B. R. Wood, L. Chiriboga, H. Yee, M. A. Quinn, D. McNaughton and M. Diem, *Gynecologic oncology*, 2004, **93**, 59-68.
133. M. Jackson, L. P. Choo, P. H. Watson, W. C. Halliday and H. H. Mantsch, *Biochimica et biophysica acta*, 1995, **1270**, 1-6.

134. M. Diem, S. Boydston-White and L. Chiriboga, *App. Spectrosc.*, 1999, **53**, 148A-161A.
135. M. Diem, M. Romeo, S. Boydston-White, M. Miljkovic and C. Matthaus, *The Analyst*, 2004, **129**, 880-885.
136. B. Mohlenhoff, M. Romeo, M. Diem and B. R. Wood, *Biophys J*, 2005, **88**, 3635-3640.
137. C. Lengauer, K. W. Kinzler and B. Vogelstein, *Nature*, 1998, **396**, 643-649.
138. B. R. Wood, K. R. Bambery, P. Heraud and D. McNaughton, in *FT-IR Spectroscopy in Microbiological and Medical Diagnostics*, eds. D. Naumann and P. Lasch, Robert Koch Institute, Berlin, 2009.
139. D. R. Whelan, K. R. Bambery, L. Puskar, D. McNaughton and B. R. Wood, *The Analyst*, 2013, **138**, 3891-3899.
140. D. R. Whelan, K. R. Bambery, L. Puskar, D. McNaughton and B. R. Wood, *Journal of biophotonics*, 2013, **6**, 775-784.
141. H. Zentgraf, D. Duemling and W. W. Franke, *Exp.Cell Res.*, 1969, **56**, 333–340
142. Z. Nie, F. Cui, Y. K. Tzeng, H. C. Chang, M. Chu, H. C. Lin, C. H. Chen, H. H. Lin and A. L. Yu, *Anal. Chem.*, 2007, **79**, 7401–7407.
143. C. Hughes, M. D. Brown, F. J. Ball, G. Monjardez, N. W. Clarke, K. R. Flower and P. Gardner, *The Analyst*, 2012, **137**, 5736-5742.
144. D. E. Bedolla, S. Kenig, E. Mitri, P. Ferraris, A. Marcello, G. Grenci and L. Vaccari, *The Analyst*, 2013, **138**, 4015-4021.
145. S. Boydston-White, T. Gopen, S. Houser, J. Bargonetti and M. Diem, *Biospectroscopy*, 1999, **5**, 219-227.
146. A. Derenne, A. Mignolet and E. Goormaghtigh, *The Analyst*, 2013, **138**, 3998-4005.
147. H. Y. Holman, M. C. Martin, E. A. Blakely, K. Bjornstad and W. R. McKinney, *Biopolymers*, 2000, **57**, 329-335.
148. M. Jimenez-Hernandez, M. D. Brown, C. Hughes, N. W. Clarke and P. Gardner, *The Analyst*, 2015, **140**, 4453-4464.
149. M. Jimenez-Hernandez, C. Hughes, P. Bassan, F. Ball, M. D. Brown, N. W. Clarke and P. Gardner, *The Analyst*, 2013, **138**, 3957-3966.
150. F. Q. Zhang, J. Qi and Z. G. Yang, *Guang pu xue yu guang pu fen xi = Guang pu*, 2011, **31**, 2076-2080.
151. S. Boydston-White, M. Romeo, T. Chernenko, A. Regina, M. Miljkovic and M. Diem, *Biochimica et biophysica acta*, 2006, **1758**, 908-914.
152. P. L. Fale, A. Altharawi and K. L. Chan, *Biochimica et biophysica acta*, 2015, **1853**, 2640-2648.
153. P. Bassan, A. Sachdeva, A. Kohler, C. Hughes, A. Henderson, J. Boyle, J. H. Shanks, M. Brown, N. W. Clarke and P. Gardner, *The Analyst*, 2012, **137**, 1370-1377.

Figure captions

Figure 1. X-ray diffraction pattern showing how the reciprocal distances and angles define the actual distances and angle in the structure of B-DNA.

Figure 2. Molecular models of A, B and Z-DNA.

Figure 3. Schematic showing the DNA double helix with some of the critical parameters that define the B-form showing the major and minor groove and the important distances and angles. Modified version of figure appearing in reference 7 with permission from Elsevier Books.

Figure 4. CaF_2 windows with fabricated spacers for assembly into ThermoFisher compression cell. (A) First design spacer pattern with single outlet channel. (B) Revised spacer pattern. (C) and (D) Cleaning and assembly of custom CaF_2 windows into compression cell. Reproduced from reference 42 with permission from Elsevier.

.

F**igure 5. (Top panel)** Spectral series for pure reference samples: (A) Single stranded DNA dehydrating (T-FTIR), (B) Single stranded RNA rehydrating (ATR-FTIR), (C) Double stranded DNA dehydrating (T-FTIR), and (D) Double stranded DNA dehydrating (T-FTIR). In all spectral series red denotes dehydrated, blue denotes hydrated. (**Bottom panel)** Second derivative spectral series for pure reference samples: (A) Single stranded DNA dehydrating (T-FTIR), (B) Single stranded RNA rehydrating (ATR-FTIR), (C) Double stranded DNA dehydrating (T-FTIR), and (D) Double stranded DNA dehydrating (T-FTIR). In all spectral series red denotes

dehydrated, blue denotes hydrated. Reproduced from reference 40 with permission of Oxford University Press.

Figure 6. ATR spectra recorded of air-dried chicken (nucleated) and human (anucleated) erythrocytes showing the close similarity of spectra in the phosphodiester region (1300-800 cm^{-1}). Reproduced from reference 100 with permission from Elsevier.

Figure 7. FTIR transmission spectra recorded of chicken erythrocytes as a function of hydration. The arrows highlight the DNA bands that radically change during hydration. Reproduced from reference 90 with permission from Springer.

Figure 8. Top panel T-FTIR rehydration spectral series of mammalian lymphocytes. **Bottom panel** Calculated second derivative series. In all spectral series red denotes dehydrated, blue denotes hydrated. Reproduced from reference 40 with permission from Oxford University Press.

Figure 9. A. Schematic of the eukaryotic cell cycle showing the time marked as M for approximate synchronization time with M + x indicating approximate measurement times. **B.** Spectra of live synchronised cells after vector normalization showing dramtic changes in the 1300-1000 cm^{-1} for the M + 11 to M + 21 time points. **C.** PCA scores plot (PC1 versus PC2) showing spectra recorded of cells from three independent synchronised cultures. The cells have grouped clearly together for the different time points M+1 and M+3 showing the high reproducibility that can be achieved uisng synchonised cultures and analysing single cells using a synchotron

light source. Reproduced from Ref. 104 with permission from the Centre National de la Recherche Scientifique (CNRS) and The Royal Society of Chemistry.

Figure 10. FTIR spectra (A) and calculated second derivatives (B) of *Escherichia coli* in the dormant dehydrated state (red) and after rehydration (blue). From left to right, shading highlights the characteristic antisymmetric phosphate stretch, the symmetric phosphate stretch, and the backbone carbon-carbon vibration that are diagnostic of the A to B-DNA transition. Reporduced from reference 20 under the Creative Commons (CC BY 4.0).

Table 1. Structural parameters of the main DNA conformations

Structural Parameter	A-DNA	B-DNA	Z-DNA
Direction of helix rotation	Right handed	Right handed	Left handed
Residue per helical turn	11	10.5	12
Axial rise per residue	0.255 nm	0.34 nm	0.37 nm
Pitch (length) of the helix	2.82 nm	3.4 nm	4.44 nm
Base pair tilt	20°	-6°	7°
Rotation per residue	32.7°	34.3°	-30°
Diameter of helix	2.3 nm	2.0 nm	1.8 nm
Nucleotide phosphate distance	0.59 nm	0.7 nm	C: 5.7 nm G: 6.1 nm
Configuration dA, dT, dC	anti	anti	anti
of glycosidic bond dG	anti	anti	syn
Sugar Pucker dA, dT, dC	C3' endo	C2' endo	C2' endo
dG	C3' endo	C2' endo	C3' endo

Table 2. Major bands found in cells, tissues and nucleic acids

Wavenumber (cm^{-1})	**Assignment**
3600-3500	Amide A, Proteins, ν(N-H)
3490	Water, ν_3, $\nu_{as}OH$
3277	Water, ν_2, $\nu_{as}OH$
2956	$\nu_{as}CH_3$ acyl chains lipids
2922	$\nu_{as}CH_2$ acyl chains lipids
2874	ν_sCH_3 acyl chains lipids
2852	ν_sCH_2 acyl chains lipids
1740	Lipids, ν(C=O) ester carbonyl
1715	B-DNA base pairing vibration (**ν**C=O & **ν**C=N)
1708	A-DNA base pairing vibration (**ν**C=O & **ν**C=N)
1720-1666	νC=O from purine and pyrimidine
1695	Z-DNA base pairing vibration (**ν**C=O & **ν**C=N)
1690	RNA, ν_a (C_2=O)
1660-1665	DNA, **ν**(C_5=O), **δ**(N=H), RNA, **ν**(C6=O)
1650	Amide I, Protein, α-helical
1635	Amide I, Proteins, β-pleated sheet
1642	Water, ν_2 , $\delta(H_2O)$,
1610	DNA and RNA, **ν**C_4=C5 imidazole
1605	DNA, δNH_2
1578	DNA and RNA, **ν**C=N imidazole ring
1545-1530	Proteins, amide II
1418, 1425, 1408	A-DNA, B-DNA, Z-DNA Deoxyribose
1457	$\delta_{as}CH_3$ of cellular proteins
1450	Proteins, lipids, **δ**CH_2
1400	**ν**COO^-_2 of fatty acids and amino acid side chains
1300-1250	Proteins, amide III
1244	RNA, $\nu_{as}PO_2^-$
1240, 1225, 1215	A-DNA, B-DNA, Z-DNA, ν_{as} PO_2^-
1185	A-DNA, Ribose
1160, 1120	RNA, **ν**(C=O) ribose
1080	DNA, $\nu_sPO_2^-$
1060, 1050	DNA, RNA, ν(C-O) ribose
1038	RNA, **ν**(C=O) ribose
1015	DNA and RNA, ν(C-O) ribose
1014-1018	Z-DNA marker band
996	RNA, uracil ring motions
970, 915	DNA, RNA, ribose-phosphate skeletal motions
899, 894, 929	A-DNA, B-DNA, Z-DNA
806, 830-840	A-DNA, B-DNA

Figure 1

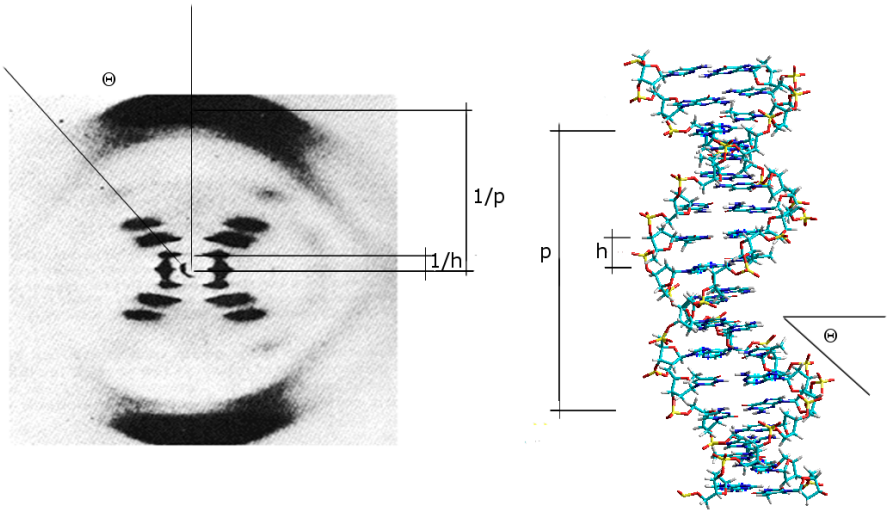

Figure 2

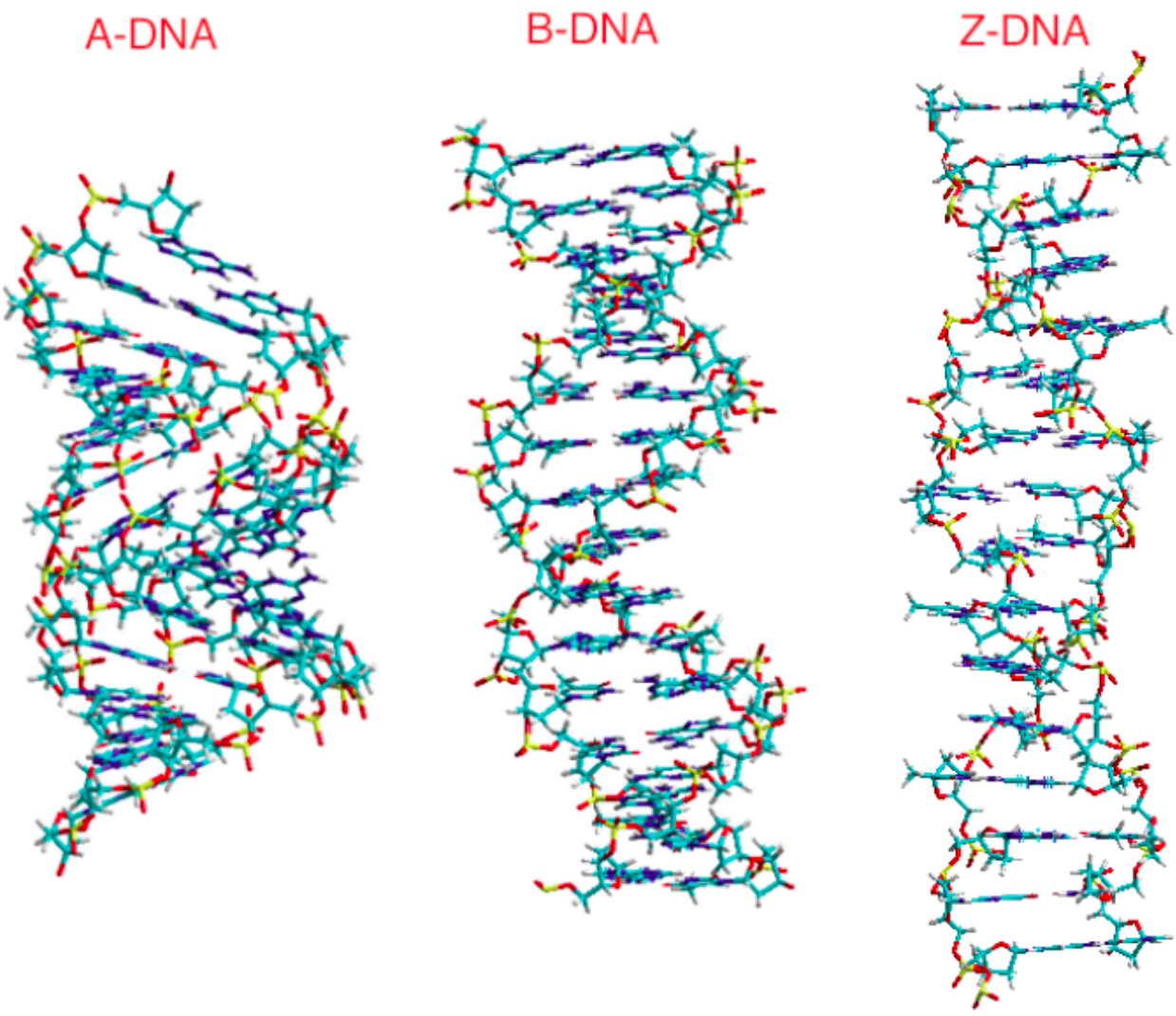

Figure 3

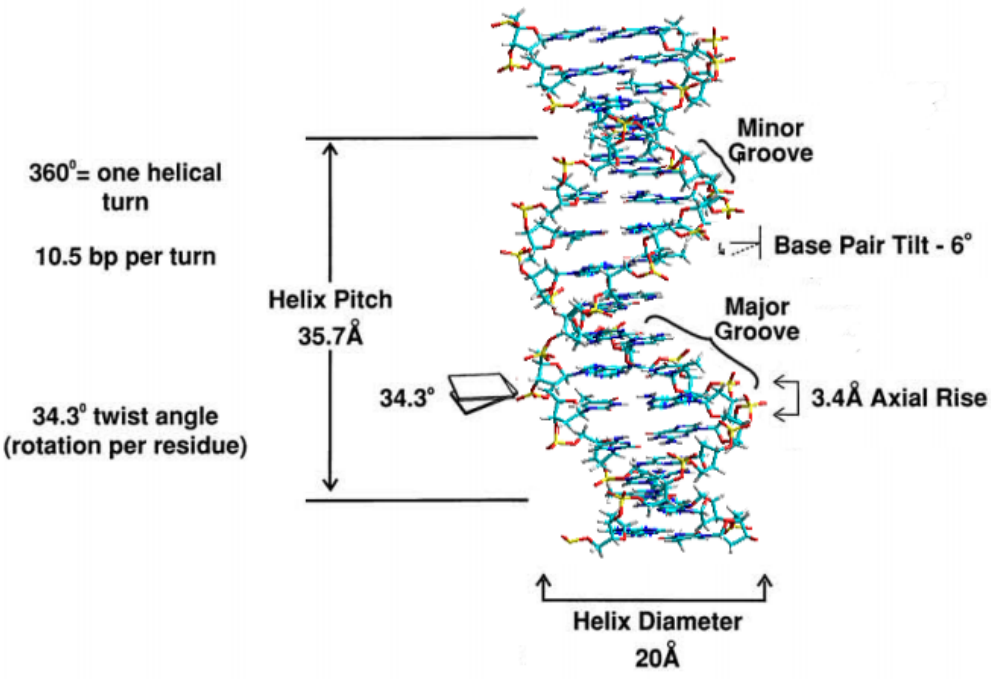
360°= one helical turn
10.5 bp per turn
Helix Pitch 35.7Å
34.3° twist angle (rotation per residue)
Minor Groove
Base Pair Tilt - 6°
Major Groove
34.3°
3.4Å Axial Rise
Helix Diameter 20Å

Figure 4

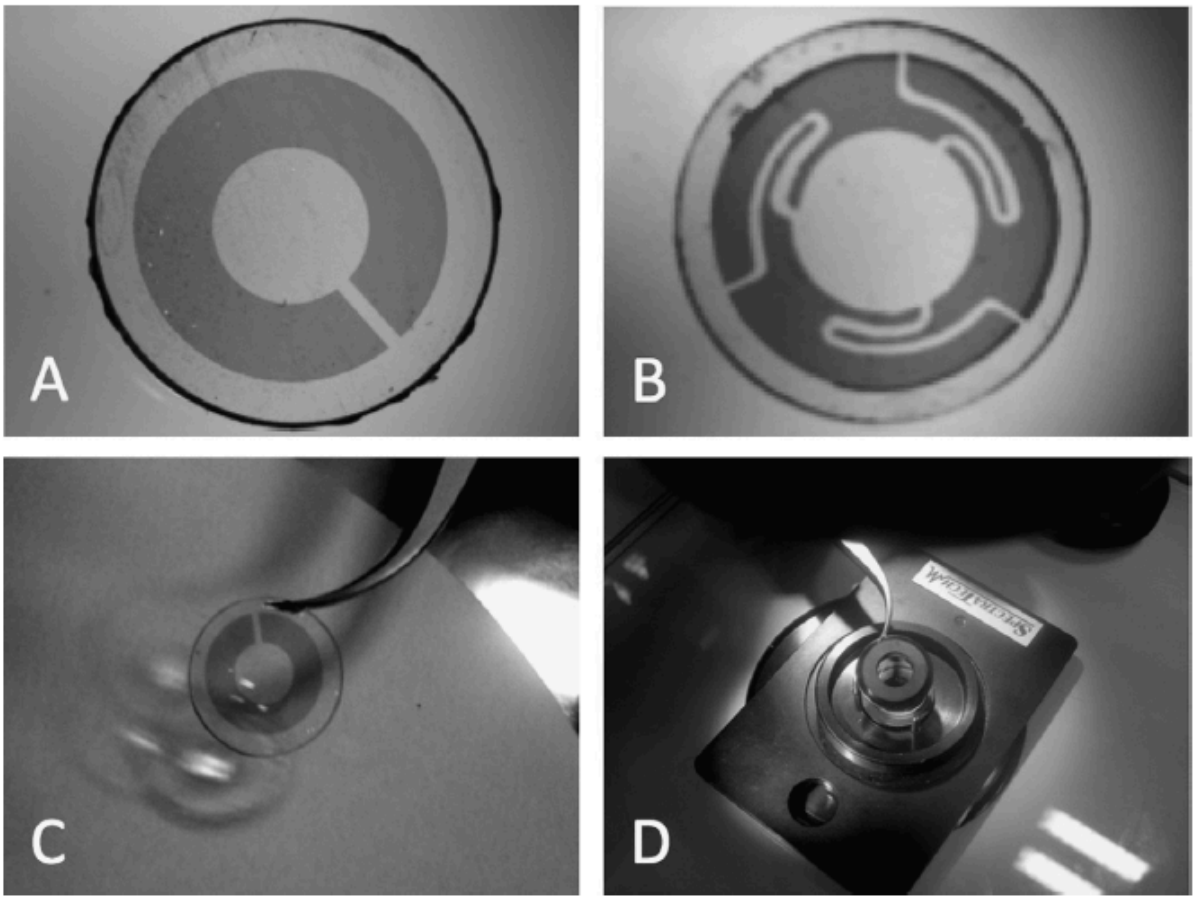

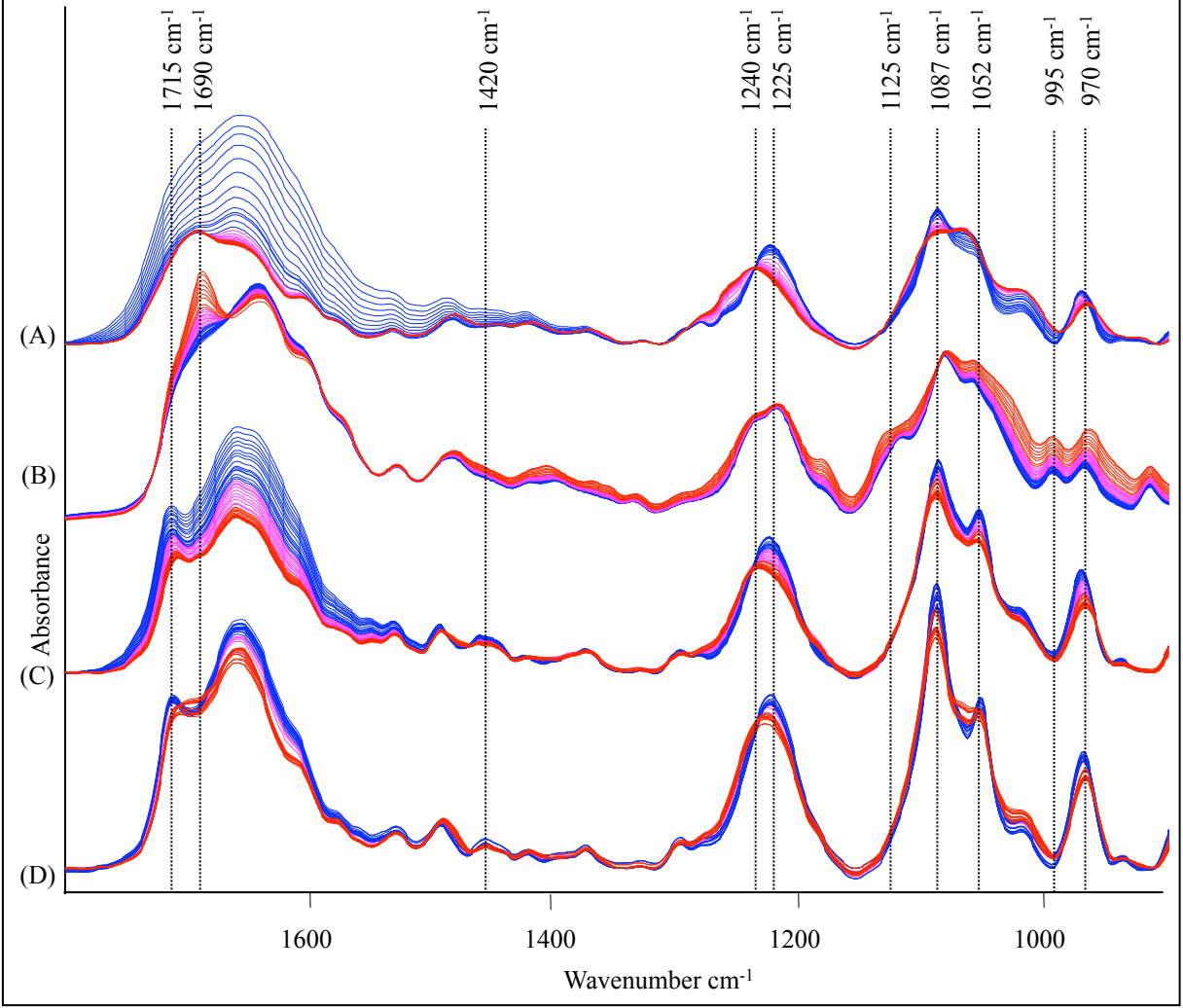
1715 cm-1
1690 cm-1
1420 cm-1
1240 cm-1
1225 cm-1
1125 cm-1
1087 cm-1
1052 cm-1
995 cm-1
970 cm-1
(A)
(B)
(C)
(D)
Absorbance
1600
1400
1200
1000
Wavenumber cm-1

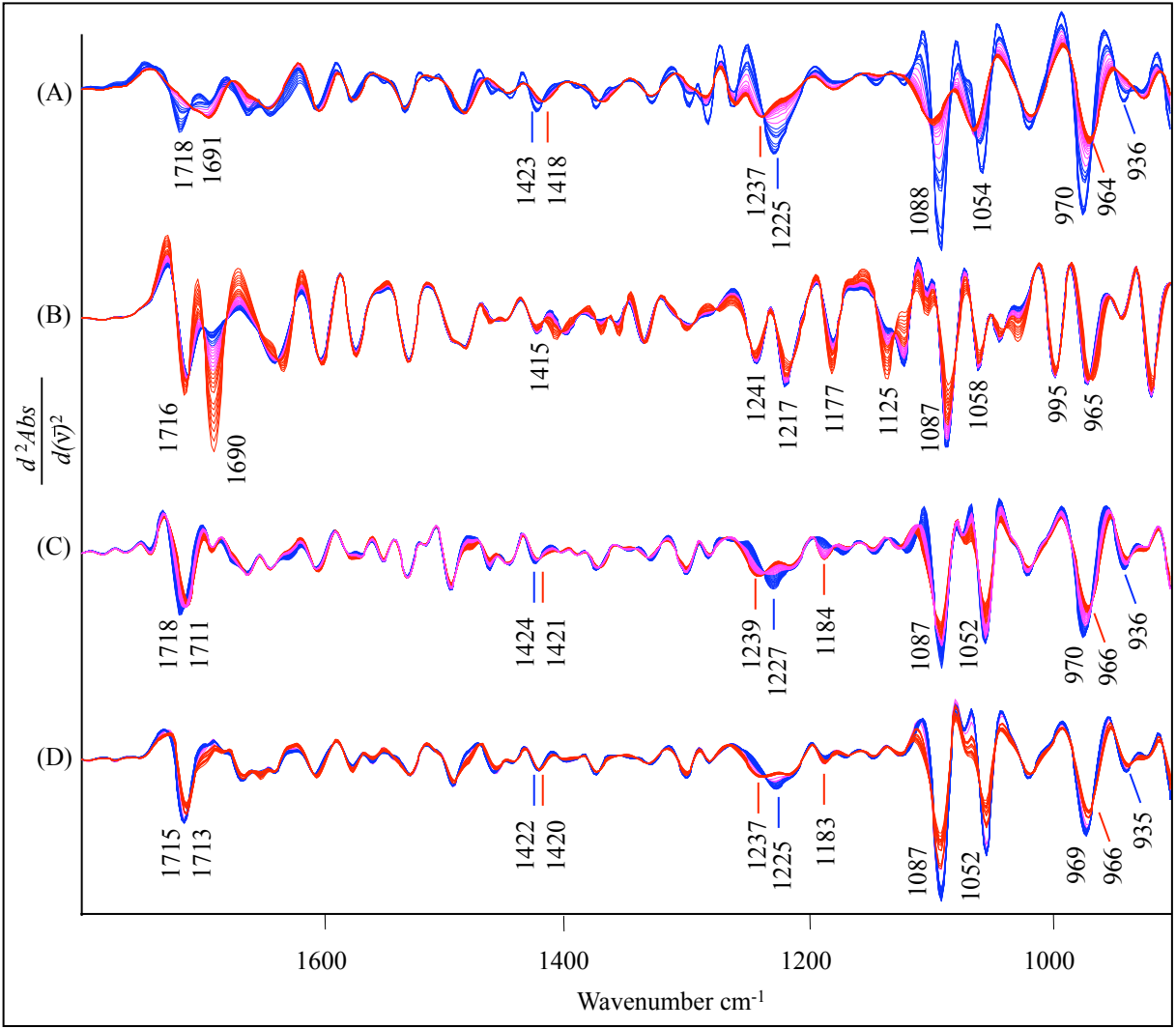
(A)
1718
1691
1423
1418
1237
1225
1088
1054
970
964
936
(B)
1716
1690
1415
1241
1217
1177
1125
1087
1058
995
965
(C)
1718
1711
1424
1421
1239
1227
1184
1087
1052
970
966
936
(D)
1715
1713
1422
1420
1237
1225
1183
1087
1052
969
966
935
$\frac{d^2Abs}{d(\tilde{\nu})^2}$
1600
1400
1200
1000
Wavenumber cm^{-1}

Figure 6

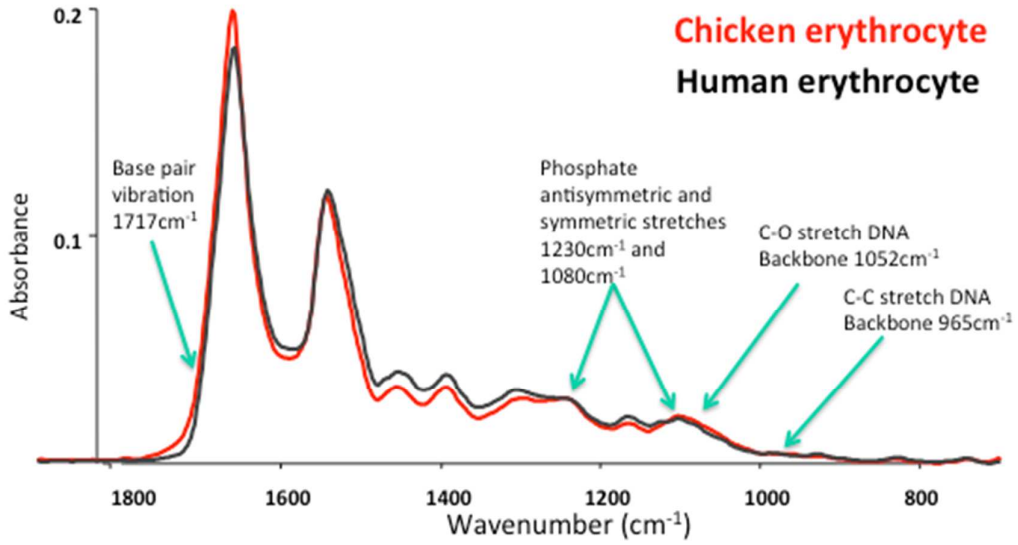
Chicken erythrocyte
Human erythrocyte
Base pair vibration 1717cm-1
Phosphate antisymmetric and symmetric stretches 1230cm-1 and 1080cm-1
C-O stretch DNA Backbone 1052cm-1
C-C stretch DNA Backbone 965cm-1
Absorbance
0.2
0.1
1800
1600
1400
1200
1000
800
Wavenumber (cm-1)

Figure 6

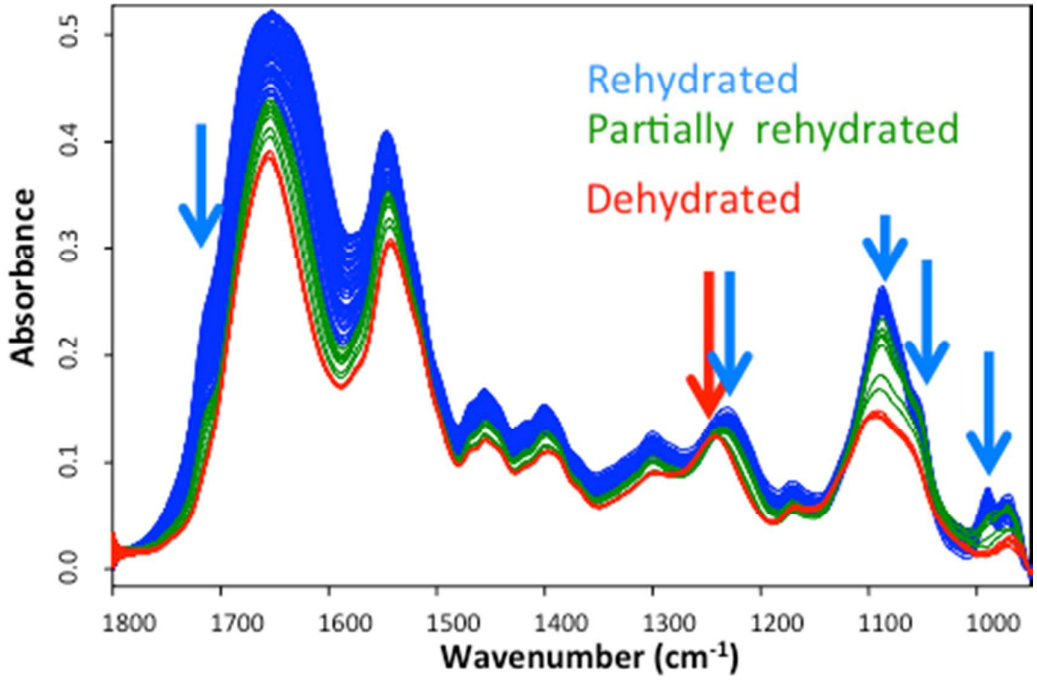
Rehydrated
Partially rehydrated
Dehydrated
Absorbance
0.0
0.1
0.2
0.3
0.4
0.5
1800
1700
1600
1500
1400
1300
1200
1100
1000
Wavenumber (cm-1)

Figure 8

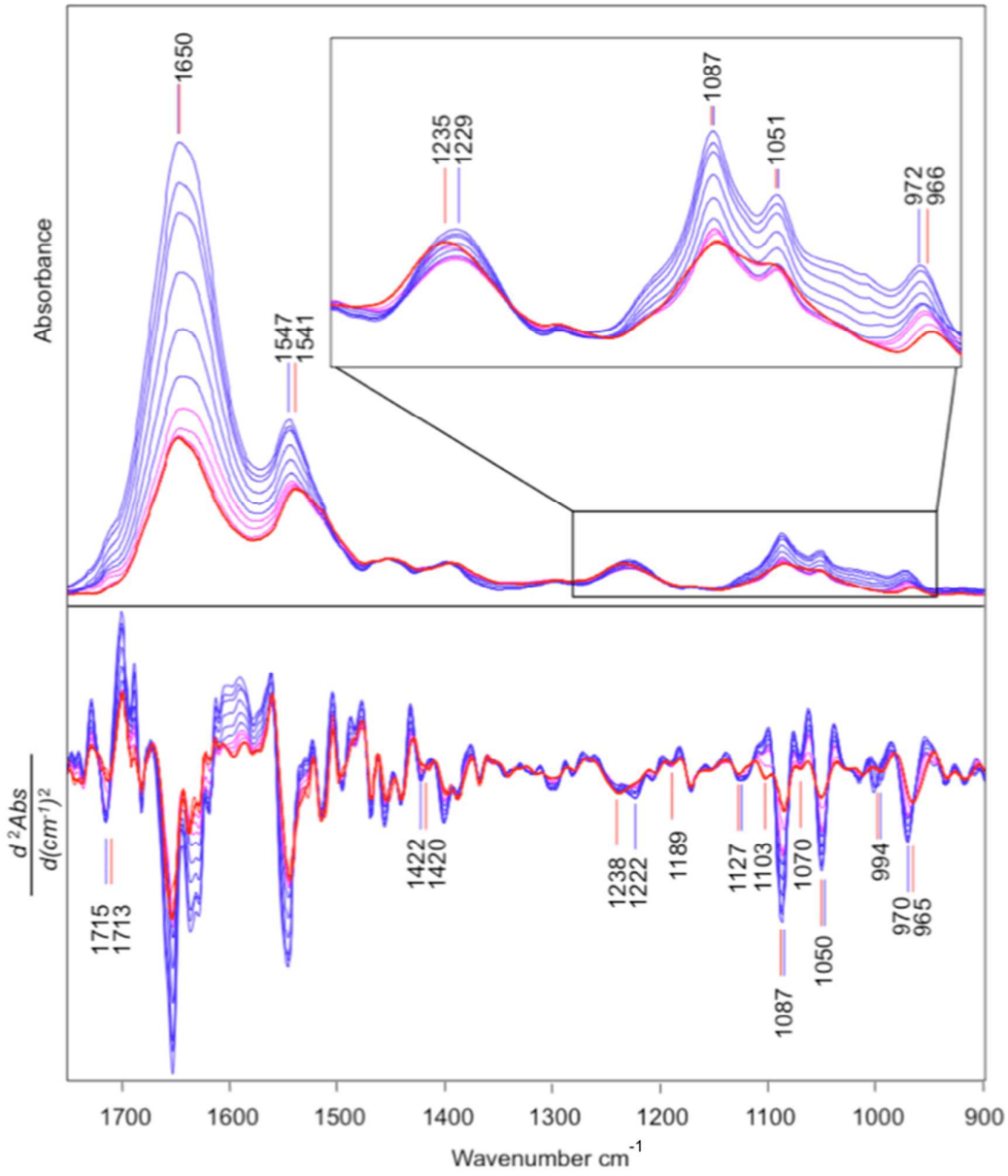
1650
1547
1541
1235
1229
1087
1051
972
966
Absorbance
1715
1713
1422
1420
1238
1222
1189
1127
1103
1070
1087
1050
994
970
965
d²Abs / d(cm⁻¹)²
1700
1600
1500
1400
1300
1200
1100
1000
900
Wavenumber cm⁻¹

Figure 9

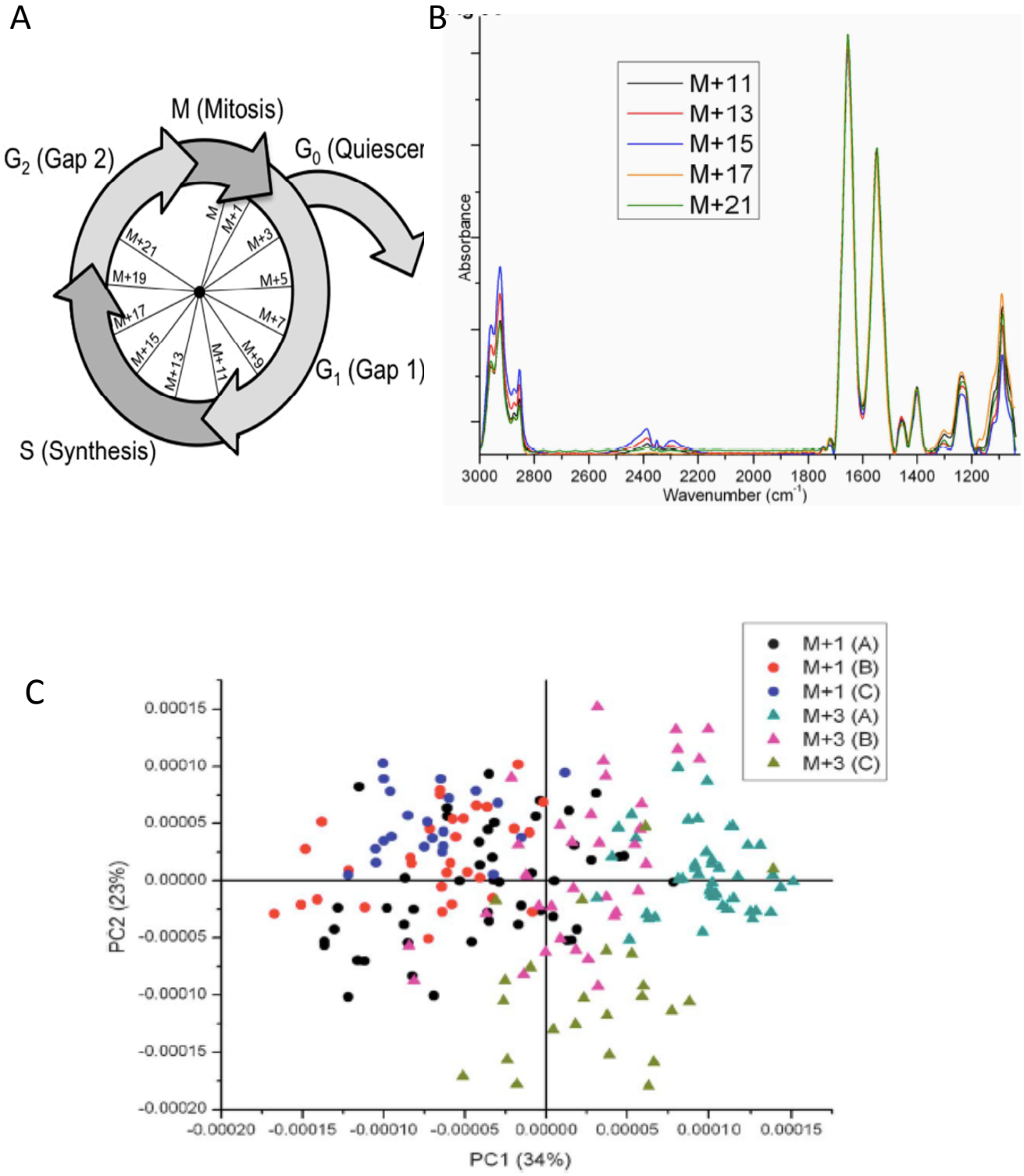
A
M (Mitosis)
G2 (Gap 2)
G0 (Quiescer
G1 (Gap 1)
S (Synthesis)
M
M+1
M+3
M+5
M+7
M+9
M+11
M+13
M+15
M+17
M+19
M+21
B
M+11
M+13
M+15
M+17
M+21
Absorbance
3000 2800 2600 2400 2200 2000 1800 1600 1400 1200
Wavenumber (cm-1)
C
M+1 (A)
M+1 (B)
M+1 (C)
M+3 (A)
M+3 (B)
M+3 (C)
PC2 (23%)
0.00015
0.00010
0.00005
0.00000
-0.00005
-0.00010
-0.00015
-0.00020
-0.00020 -0.00015 -0.00010 -0.00005 0.00000 0.00005 0.00010 0.00015
PC1 (34%)

Figure 10

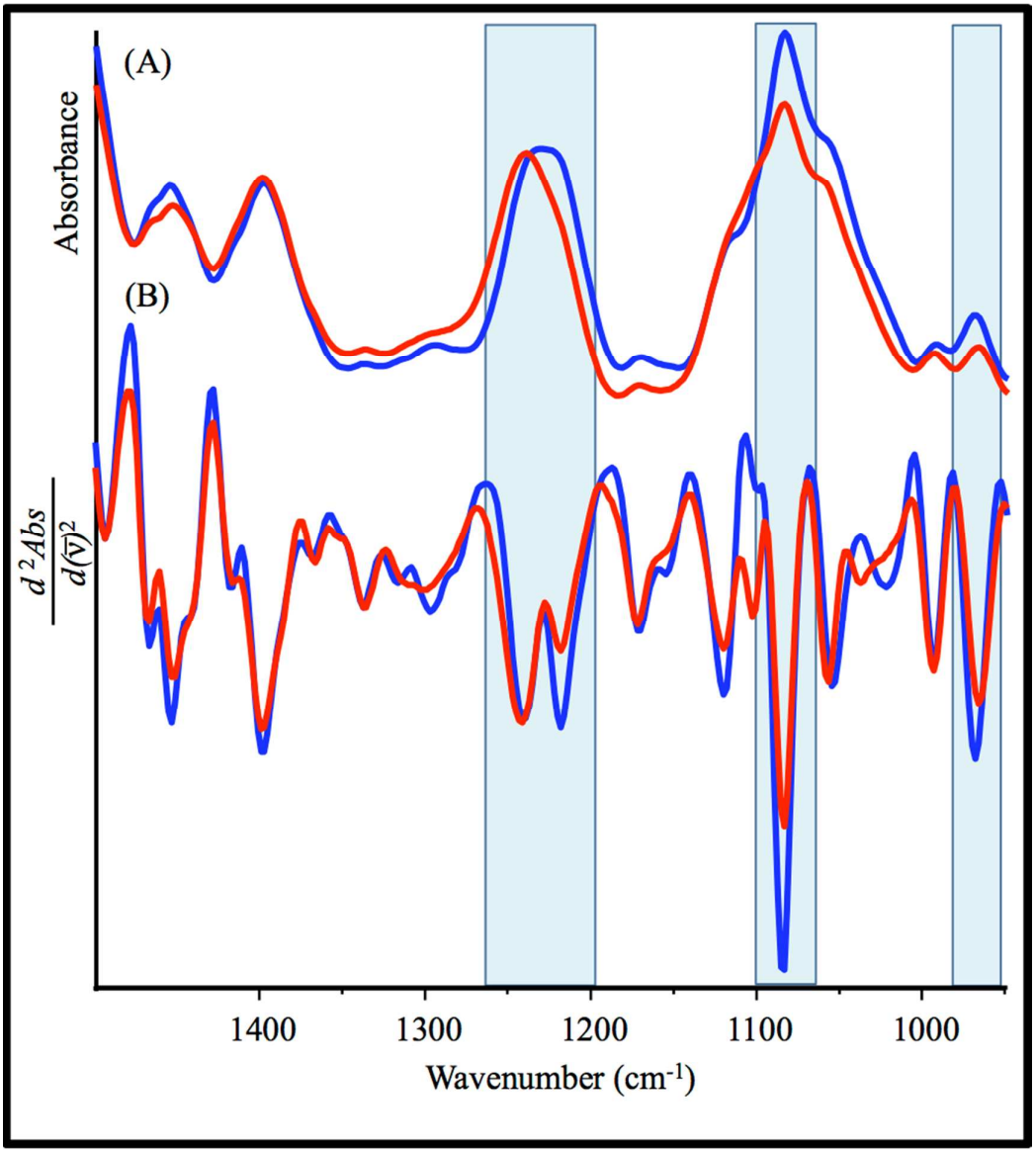
(A)
Absorbance
(B)
$\frac{d^2Abs}{d(\bar{\nu})^2}$
1400
1300
1200
1100
1000
Wavenumber (cm^{-1})